https://doi.org/10.5194/esurf-2021-8
Preprint. Discussion started: 23 February 2021

Earth Surface Dynamics Discussions
Open Access
EGU

Validation and application of sequential unmanned aerial vehicle surveys to monitor the kinematics of a rapid rock glacier

Sebastián Vivero[1], Reynald Delaloye[2], Christophe Lambiel[1]

[1]Institute of Earth Surface Dynamics, University of Lausanne, Lausanne, 1015, Switzerland
[2]Department of Geosciences/Geography, University of Fribourg, Fribourg, 1700, Switzerland

Correspondence to: Sebastián Vivero (sebastian.viveroandrade@unil.ch)

Abstract.

Accurately assessing landform evolution and quantifying rapid environmental changes are gaining importance in the context of monitoring techniques in alpine environments. In the European Alps, glaciers and rock glaciers are among the most characteristic cryospheric components bearing the most prolonged monitoring periods. This study introduces a rigorous procedure to quantify rock glacier kinematics and their associated uncertainty derived from sequential unmanned aerial vehicle (UAV) surveys. High-resolution digital elevation models (DEMs) and orthomosaics are derived from UAV image series combined with structure from motion (SfM) photogrammetry techniques. Multitemporal datasets are employed for measuring spatially continuous rock glacier kinematics using image matching algorithms. This procedure is tested on seven consecutive (from 2016 to 2019) UAV surveys of Tsarmine rock glacier, Valais Alps, Switzerland. The evaluation of superficial displacements was performed with simultaneous in-situ differential global navigation satellite system (GNSS) measurements. During the study period, the rock glacier doubled its overall frontal velocity, from around 5 m yr^{-1} between October 2016 and June 2017 to more than 10 m yr^{-1} between June and September 2019. Using the adequate UAV survey acquisition, processing, and validation steps, we almost achieved the same accuracy as the GNSS-derived velocities. Nevertheless, the proposed monitoring method provides accurate surface velocity fields values, which allow an enhanced description of the current rock glacier dynamics and its surface expression.

1 Introduction

Rock glaciers represent one of the most iconic and abundant landforms inside the mountain permafrost realm (Barsch, 1996; Jones et al., 2018). As conspicuous periglacial landforms, they have been regarded as useful indicators of past and present permafrost conditions in different mountain chains (Kellerer-Pirklbauer et al., 2008; Konrad et al., 1999; Sorg et al., 2015; Winkler and Lambiel, 2018). Rock glacier analogues have even been discovered on extra-terrestrial planetary bodies such as Mars (Hubbard et al., 2014), where ground ice is most likely abundant (Clifford et al., 2003). The dynamics of rock glaciers includes not only the acting forces on the creeping body but also the 3D changes over time (Kääb, 2005). Whereas the former cannot be directly measured by remote sensing techniques but from modelling approaches (e.g. Müller et al., 2016), the latter

https://doi.org/10.5194/esurf-2021-8
Preprint. Discussion started: 23 February 2021


Earth Surface Dynamics Discussions Open Access EGU

(i.e. kinematics) can be monitored by different remote sensing and in-situ measurements (Haeberli et al., 2006). As such, superficial displacements are expected to reflect mainly the creep of the permafrost body inside the rock glacier (Arenson et al., 2002). This creeping process is dominated by the high deformation rate at the shear horizon, which accommodates a large portion of the observable surface displacement (60%–90%) and it is usually located at a depth of 10 to 30 m from the top (Arenson et al., 2002; Cicoira et al., 2020; Haeberli et al., 2006; Krainer et al., 2015; Wagner, 1992).

Rock glacier kinematics are commonly derived from consecutive acquisition epochs, forming different time series of seasonal, annual, and decadal observation periods (Delaloye et al., 2010; Kääb et al., 2007). The most extended kinematic monitoring effort goes back to the summer of 1938, and since the early 1950s at regular periods, at the Outer Hochebenkar in the Ötztal Alps of Western Austria (Hartl et al., 2016; Schneider and Schneider, 2001). Subsequently, systematic kinematic monitoring programs were initiated in 1979 at the Laurichard rock glacier in the French Alps (Bodin et al., 2009; Francou and Reynaud, 1992); and in 1995 at the Dösen rock glacier in the Hohe Tauern Range of the central Austrian Alps (Kaufmann, 2016; Kellerer-Pirklbauer et al., 2017). In the Swiss Alps, and under the coordination of the Swiss Permafrost Monitoring Network (PERMOS) continuous long-term kinematics data series are obtained for several rock glaciers, since early as 1994 at the Gemmi/Furggentälti rock glacier (PERMOS, 2019a). These time series consist mainly of data from annual surveys, providing a full and updated picture of the overall state of rock glacier kinematics. The wealth of such systematic observations have revealed strong correlations of relative velocities changes on an interannual basis for a majority of rock glaciers, and consequently, their association with changes in the thermal state of permafrost (Delaloye et al., 2008; Kellerer-Pirklbauer et al., 2018; Roer et al., 2005).

Reported rock glacier superficial velocities have ranged from a few centimetres to some metres per year (Barsch, 1996; Delaloye et al., 2010; Janke et al., 2013), but, for very fast rock glaciers, the velocities can reach several metres per year (Hartl et al., 2016; Valenzuela, 2004) or more (Delaloye et al., 2013; Eriksen et al., 2018). In the more spectacular cases, evidence of anomalous velocities or surface disturbances (e.g. cracks, crevasses and scarps) have been identified as evident signs of landform destabilisation (Roer et al. 2008; Delaloye et al., 2013; Marcer et al., 2019, 2020; Vivero and Lambiel, 2019). In this context, the main factors of rock glacier acceleration and destabilisation have been attributed to permafrost degradation due to increased atmospheric warming (Bodin et al., 2017; Deline et al., 2015; Roer et al., 2005, 2008), and by related feedback mechanisms such as increasing water content (Buchli et al., 2018; Cicoira et al., 2019; Ikeda et al., 2008; Wirz et al., 2016). Likewise, mechanical overload caused by rockfalls deposits (Delaloye et al., 2013; Scotti et al., 2017) or artificial overload by mining waste deposits (Valenzuela, 2004) have also been identified as triggers of rock glacier destabilisation.

The quantification of rock glacier movement has been traditionally measured by ground surveying techniques such as theodolite or total station instruments (Francou and Reynaud, 1992; Koning and Smith, 1999), and more recently using differential GPS (Berthling et al., 1998), differential real-time kinematic (RTK) GPS (Lambiel and Delaloye, 2004) and

https://doi.org/10.5194/esurf-2021-8
Preprint. Discussion started: 23 February 2021


Earth Surface Dynamics Discussions
Open Access
EGU

permanent GPS stations (Buchli et al., 2018; Wirz et al., 2016). Nevertheless, remote sensing techniques such as photogrammetry, high-resolution optical satellite imagery, satellite radar interferometry (InSAR) and airborne laser scanning (ALS) have become more broadly employed in recent years, mainly due to their ability to monitor vast and remote regions (Blöthe et al., 2020; Bollmann et al., 2015; Groh and Blöthe, 2019; Necsoiu et al., 2016; Rignot et al., 2002; Strozzi et al., 2020). Since the earliest examples of permafrost creep measurements extracted from analogue photogrammetry (e.g. Messerli and Zurbuchen, 1968), the quality and availability of remote sensing datasets have allowed a substantial evolution to be achieved in rock glacier research (Kääb, 2005; Kääb et al., 1997; Kääb and Vollmer, 2000).

The rapid development of Unmanned Aerial Vehicles (UAV) systems has opened up significant new applications in the field of remote sensing due to their comparably lower prices and high customised settings (Carbonneau and Dietrich, 2017; Cook, 2017; Nex and Remondino, 2014). Alongside, new developments in the domain of image processing and photogrammetric techniques, such as Structure-for-motion (SfM), have burgeoned during the last years (James and Robson, 2012; Smith et al., 2016; Westoby et al., 2012). As such, the so-called UAV-SfM workflows have been used in different domains, such as the monitoring of landslide kinematics (Clapuyt et al., 2017; Lucieer et al., 2013) and for studying glacial (Benoit et al., 2019; Rossini et al., 2018; Ryan et al., 2015) and periglacial processes (Eichel et al., 2020; Hendrickx et al., 2020), among other applications. Until now, only a few study cases analyses the benefits of UAV-SfM techniques for rock glacier monitoring (Dall'Asta et al., 2017; Fey and Krainer, 2020; Vivero and Lambiel, 2019). However, as UAV systems are continuously changing and improving, there is still scope for validation and protocol optimisation using different UAV configurations in high and challenging terrain.

The broad range of rock glacier surface velocities (from few centimetres to several metres per year) makes a robust validation of these magnitudes obtained from particular remote sensing techniques necessary. Likewise, systematic ground validation through consecutive periods is required to improve the kinematic data quality and shed light on rock glaciers' kinematic behaviour on great spatial detail. The aims of this study are twofold: (1) to investigate the benefits of high-resolution UAV surveys to study landform-wide kinematics; and (2) to evaluate the quality of this methodological approach employing highly accurate kinematic data obtained from terrestrial geodetic surveys (TGS). To achieve this, we have performed repeated and simultaneous UAV, and global navigation satellite system (GNSS) surveys at the Tsarmine rock glacier (Swiss Alps) since 2016. The workflow presented allows for gaining high-quality rock glacier kinematic data, which helps to understand the current rock glacier dynamic behaviour better. We propose that repeated UAV surveys provide complementary information to improve our understanding of rock glacier kinematics and dynamics, and therefore, a potential technique to be integrated into the mountain permafrost monitoring programs.

https://doi.org/10.5194/esurf-2021-8
Preprint. Discussion started: 23 February 2021


Earth Surface Dynamics Discussions
Open Access
EGU

2 Material and methods

2.1 Site description

The Tsarmine rock glacier (46°02' N, 7°30' E) is located in the Arolla Valley, Western Swiss Alps (see Lambiel, 2021). The morphology corresponds to a long tongue-shaped form, displaying 550 m long and 120 m wide, and with an altitudinal range between 2470 (terminus) and 2700 (rooting zone) m a.s.l. (Fig 1). This active landform sits close to the regional lower limit of discontinuous permafrost in the area (Deluigi et al., 2017). Furthermore, geoelectrical surveys on the rock glacier and its connecting talus slope indicate that the active layer thickness ranges between 3 to 5 m, whereas the frozen body thickness reaches 15 m at least (Lambiel, 2006).

Sub-metric rocks to metric-sized boulders from an orthogneiss lithology (Arolla series) are abundant on the surface ('bouldery rock glacier' sensu Ikeda and Matsuoka, 2006), whereas finer matrix sediments are visible at the steep front (Fig 1). Webcam images indicate that the main shear horizon is about 15 m below the front line edge (Kummert et al., 2018). Due to the absence of compression, the rock glacier surface is devoid of the "classical" ridge and furrow morphology (Frehner et al., 2015), but it displays protruding lateral margins or levees (Fig 1). Based on terrestrial laser scanning (TLS) surveys, Micheletti et al. (2016) indicated that between 2014 and 2015 the rock glacier terminus was providing sediments to the downstream gully in the order of ~ 1500 m^3 yr^{-1}. Subsequently, and based on TLS surveys, Kummert and Delaloye (2018) calculated that between 2015 and 2016, the sediment transfer rate was about 3500 m^3 yr^{-1}. For the last years, sediment transfer rates have progressively risen to more than 10,000 m^3 yr^{-1} (unpublished data).

Based on the analysis of archival aerial imagery Micheletti et al. (2015) showed an acceleration of this landform from 0.3 to more than 2 m yr^{-1} between 1967 and 2005. Between the beginning of the TGS measurements in 2004 and until 2012, mean annual surface velocities where around 2 m yr^{-1} (PERMOS, 2013). More recent TGS reveal a marked acceleration, with velocities of 4 m yr^{-1} between 2014 and 2016, and with peaks up to 6 m yr^{-1} in 2016 (PERMOS, 2019a). In 2019/20, annual velocities have overpassed 12 m yr^{-1} (unpublished data). Additionally, a permanent mono-frequency GNSS station with hourly resolution captured a peak monthly velocity of up to 22 m yr^{-1} in October 2020 (unpublished data). Such high velocities are a clear sign of rock glacier destabilisation (Delaloye et al., 2010; Roer et al., 2008), and therefore, their development since the early 2010s is no more fitting with the behaviour of the ensemble of rock glaciers velocities in this part of the Swiss Alps (PERMOS, 2019a). Aside from TGS surveys, monitoring activities performed in conjunction between the universities of Fribourg (UNIFR) and Lausanne (UNIL) also include the monitoring of ground surface temperatures, hourly acquisition of images by webcam devices (Kummert et al., 2018) and biannual TLS surveys of the rock glacier terminus and the subjacent gully since 2013 (Kummert and Delaloye, 2018).

https://doi.org/10.5194/esurf-2021-8
Preprint. Discussion started: 23 February 2021


Earth Surface Dynamics Discussions
Open Access
EGU

126 **2.2 Terrestrial geodetic surveys**

127 The rock glacier kinematics have been measured biannually (early summer and autumn) at around 58 points distributed along
128 sub-parallel lines since 2004 (Fig. 1). Additionally, six fixed points on stable terrain outside the rock glacier are measured
129 during each survey to cross-assess the consistency of the positional error. Their position was surveyed using either a Trimble
130 R10 or a Leica GS10 differential GNSS setups (rover and base). The survey style follows the protocol elaborated by Lambiel
131 and Delaloye (2004), employing differential GNSS devices with RTK technique for rapid measurements over large areas. The
132 positioning error usually lies in the cm range in the horizontal coordinates but may rise to more than 2 cm in the elevation
133 component. Additionally, a Post-Processing Kinematic (PPK) treatment was conducted on the Trimble R10 raw data using
134 Trimble Business Center (TBC) v4 surveying software, linking our base station with the permanent base station in Zermatt
135 from the Automatic GNSS Network for Switzerland (AGNES). This procedure also aided to evaluate the stability of the base
136 station between 2016 and 2019.
137
138 Due to the loss of individually marked boulders at the rock glacier front and the inability to measure some markers covered by
139 snow, we procured 35 points regularly measured between October 2016 and June 2019 to validate our close-range remote
140 sensing approach. We also measured four additional permanent ground control points (GCPs) located outside the rock glacier
141 (Fig 1) and several checkpoints (CPs) during nearly each field campaign since 2017 (Table 2). The four permanent GCPs,
142 which were deployed in the field before October 2016, are employed during the UAV imagery processing for improving the
143 SfM results and for a better co-alignment between UAV and GNSS surveys (Forlani et al., 2018). Moreover, the stability of
144 those GCPs was confirmed with repeated measurements in October 2018 and September 2020.

145 **2.3 UAV surveys**

146 The operation of UAV systems is often challenging in steep mountainous terrain. The UAV device must keep an elevation
147 above the ground low enough to have a good high ground sampling density, but safe enough to avoid a potential collision with
148 obstacles. Since October 2016 and simultaneously to the GNSS surveys, seven UAV surveys were deployed using a
149 lightweight SenseFly eBee RTK device (Table 1). This fixed-wing UAV is equipped with a built-in GNSS L1 and L2 signals
150 antenna and with the capability of RTK differential corrections employing either a GNSS base station or a virtual reference
151 station (VRS). Two digital cameras, a Sony WX 4.5 focal length (only available for 2016 survey) and a SenseFly Sensor
152 Optimised for Drone Applications (S.O.D.A.) 20 megapixel 10.5 focal length devices were employed for the ensemble of
153 UAV surveys. Nominal geo-tags using the RTK corrections stored in the image metadata are quote to achieve around 3 cm
154 horizontal and 5 cm vertical accuracy (i.e. camera positions). The UAV camera orientation values (Roll, Pitch, and Yaw angles)
155 recorded by the Inertial Measurement Unit (IMU) device have low accuracy. However, independent tests have found that
156 position accuracies are mainly too optimistic, suggesting that some sort of ground or check control should be included during
157 the UAV block orientation (Benassi et al., 2017).

https://doi.org/10.5194/esurf-2021-8
Preprint. Discussion started: 23 February 2021

158

159 UAV missions were planned and deployed using the SenseFly eMotion 3 software installed on a portable field computer. The
160 flight missions were planned with a longitudinal overlap of 80% and a side overlap of 70%, giving a mean of five overlapping
161 images for every point reconstructed throughout the surveyed area (Hendrickx et al., 2019). The VRS was configured to acquire
162 broadcasted differential corrections from the AGNES service using an RTCM 3.1 protocol. The eBee RTK was hand-launched
163 by the operator, who monitored the flight plan, observed the UAV system, and managed the landing in a small flat area with
164 alpine grass near the rock glacier. Moreover, and due to variable steep mountain terrain, each UAV survey was performed at
165 a constant elevation above the ground with the aid of the SwissALTI3D model digital elevation model (DEM) loaded in
166 eMotion 3 planning step. In our study area, this DEM has a pixel size of 2 m and a vertical accuracy of ± 1–3 m (Swisstopo,
167 2018).

168 **3 Data Processing**

169 **3.1 Surface movements from GNSS surveys**

170 Surface movements were calculated from the TGS by measuring the 2D (x and y) component of kinematic points at two
171 sequential surveys. The corresponding horizontal displacements were calculated from the *x* and *y* coordinates in terms of the
172 Revised Swiss Reference System (CH1903+ LV95) as

173 $$d = \sqrt{\Delta x^2 + \Delta y^2}, \quad (1)$$

174 where Δx and Δy are components of the horizontal displacement in easting and northing coordinates, respectively. The resulting
175 displacements were transformed to velocities in metres per year (m yr^{-1}) based on the time interval between the consecutive
176 surveys (see Table 1). During the PPK treatment of the GNSS data acquired with the Trimble R10 equipment, the standard
177 deviation errors of the *x* and *y* coordinates fluctuated between 1–3 cm, whereas errors of the *z* coordinate fluctuated between
178 1.5–4 cm. However, technical difficulties hampered PPK treatment of the raw GNSS data acquired during the TGS with the
179 LEICA GS10 equipment. Therefore, the standard deviation errors of the *x*, *y* and *z* coordinates were estimated based on the
180 surveyed positions obtained for the six fixed points (Fig. 1) during each TGS campaign. Thus, the uncertainty of each
181 displacement was calculated using a rigorous estimation of the standard deviation of d (Savšek-Safic et al., 2006) as provided
182 by

183 $$\sigma_d = \sqrt{\left(\frac{\Delta x}{d}\right)^2 \left(\sigma_{x_1}^2 + \sigma_{x_2}^2\right) + \left(\frac{\Delta y}{d}\right)^2 \left(\sigma_{y_1}^2 + \sigma_{y_2}^2\right)}, \quad (2)$$

184 where σ_x and σ_y are the individual standard deviation of each kinematic point (or their estimated global survey values), and
185 the subscripts 1 and 2 are the time of the GNSS survey acquisition.

https://doi.org/10.5194/esurf-2021-8
Preprint. Discussion started: 23 February 2021

3.2 SfM workflow

Recent improvements in photogrammetric processing capabilities, together with advances in computer vision algorithms, have facilitated the emergence of SfM with multi-view stereo (MVS) workflows. These developments have been capitalised by several open source and commercial SfM software packages, such as MicMac, Agisoft Photoscan, 3DF Zephyr and Pix4DMapper, among others (Smith et al., 2016). This study applied the SfM workflow as implemented in the commercial software Pix4DMapper Pro version 4.4 (https://pix4d.com/pix4dmapper-pro/, last access: 3 February 2020). This software provides a straightforward pipeline processing from raw images acquired by UAV devices to point cloud and orthomosaic generation through mainly three steps (Fig 2a).

Primarily, a bundle block orientation of each set of raw images (Table 2) with their corresponding geolocation information (i.e. position and orientation values) was achieved using a GNSS-supported aerial triangulation (GNSS-AT) and camera self-calibration methods (Benassi et al., 2017). The GNSS-AT consisted of using the initial geolocation information and four permanent GCP located outside the rock glacier (Figs 1 and 2) to improve the initial values for the interior and exterior orientation parameters. To compensate the geometric distortion caused by the complementary metal-oxide-semiconductor (CMOS) sensor in the Sony WX 4.5 camera (2016 UAV survey), a rolling shutter camera model was applied during the bundle block adjustment (Vautherin et al., 2016). The camera self-calibration parameters such as principal point, focal length, and radial and tangential distortion were consistent for all surveys using the same camera device. For the UAV surveys between June 2017 and June 2019, an additional set of checkpoints (CP) was employed to independently assess the quality of the bundle block orientation (Table 2). During the second step, the suitable image contrast and texture presented on the rock glacier surface facilitated the tie point extraction by feature matching algorithms with a scale-invariant feature transform (SIFT) operator (Lowe, 2004). A coarse 3-D point cloud is constructed from these tie points, and MVS methods are employed to reconstruct a densified 3-D point cloud (Carrivick et al., 2016; Smith et al., 2016). Average point densities ranged from 201 pts m^{-3} in June 2017 to 500 pts m^{-3} in June 2019. During a final step, the densified 3-D point clouds are gridded into seamless DEMs using an Inverse Distance Weighted (IDW) interpolator, whereas the ensemble of oriented images is orthorectified and mosaicked to generate a true-distance colour orthomosaics at 0.1 m pixel size.

3.3 Surface movements from sequential orthomosaics

Image matching using a normalised cross-correlation (NCC) function on CIAS software (Heid and Kääb, 2012; Kääb and Vollmer, 2000) was applied to sequential orthomosaics (obtained from the previous step) covering the Tsarmine rock glacier and its environs. This procedure relies on the heterogeneity produced by the shape and size of the boulders existent at the rock glacier surface, providing high-quality contrasting targets. Basically, the NCC matches homologous points from the rock glacier surface by correlating a window of reference pixel values (8-bit greyscale image) sampled from an initial image at time 1 with a more extensive search window area contained in an overlapping image at time 2. Cross-correlation values are

https://doi.org/10.5194/esurf-2021-8
Preprint. Discussion started: 23 February 2021

218 calculated for potential homologous points of the reference window within the search window. The homologous point that
219 obtains the highest correlation value is established to be the new point location, and therefore the 2-D displacement, from time
220 1 to time 2 (Kääb and Vollmer, 2000).
221
222 Horizontal surface displacements covering the Tsarmine rock glacier were derived from consecutive orthomosaics resampled
223 to one-tenth of the original pixel size (i.e. 0.01 m). Resampled images allowed achieving displacements at sub-pixel precisions
224 (Debella-Gilo and Kääb, 2011). Surface points for image matching were regularly spaced within the landform boundaries
225 based on a 10 m sampling grid in an Eulerian framework. We also included the 35 points from each TGS with their
226 corresponding initial coordinates as additional points for sequential CIAS calculations. A reference window (initial
227 orthomosaic) of 128 × 128 pixels and a search window (subsequent orthomosaic) of 256 × 256 pixels were found suitable to
228 compute surface displacements from few centimetres up to around thirteen metres. Before applying CIAS, the seasonal snow
229 cover was masked out due to its interference to accurately track surface boulders. Furthermore, a directional filter was used to
230 all computed vectors, considering the primary orientation and the slope gradient on the rock glacier. Nevertheless, the
231 percentage of spurious mismatches were below 5% of the total matches for all periods. An ordinary kriging interpolation was
232 applied to single data voids (i.e. one or two consecutive mismatches) for filling the data gaps in our data.
233
234 Despite using the same combination of GCPs for the sequential UAV surveys, a coregistration assessment of orthomosaic pairs
235 was performed using a Helmert similarity transform on stable sectors near Tsarmine rock glacier (Fig 1c). The delineation of
236 the stable ground was based on the previous work done by Kummert and Delaloye (2018), who thoroughly assessed three
237 stable sectors with repeated TLS surveys between 2013 and 2016 (their Fig 2). Nevertheless, TGS measurements revealed that
238 the narrow and elongated southern stable sector had moved at about 0.15 m yr^{-1} between 2016 and 2019. Therefore, this sector
239 was excluded during the coregistration assessment. Estimates of the directional variance and the systematic (bias) errors were
240 calculated for the consecutive orthomosaic pairs using around 69 stable rock surfaces circumscribed to the reassessed stable
241 sectors (Fig 1c). The Helmert similarity transform included the detection of systematic rotations, translation (*x*-*y*-shift vector),
242 and scale differences between the orthomosaics. However, we found neither scale nor rotations differences between the
243 consecutive orthomosaics, thus demonstrating the horizontal positional quality of the SfM-derived products. Removing the
244 systematic *x*-*y*-shift vector from the CIAS measurements provided a bias-free overall displacement. Similarly to Eq. (2), the
245 uncertainty of the derived horizontal displacements using CIAS can be calculated, taking into account the coregistration's
246 anisotropy in both the *x* and *y* directions (Redpath et al., 2013). Furthermore, as the Δx and Δy have been corrected for the
247 systematic (bias) coregistration errors, the standard deviation for each displacement measured by CIAS is unique and follow:

248 $$\sigma_d = \sqrt{\left(\frac{\Delta x}{d}\right)^2 \sigma_x^2 + \left(\frac{\Delta y}{d}\right)^2 \sigma_y^2}, \quad (3)$$

https://doi.org/10.5194/esurf-2021-8
Preprint. Discussion started: 23 February 2021

where σ_x and σ_y are standard deviations obtained from coregistration analysis of the stable rock surfaces using the Helmert similarity transform. In this study, we multiplied the results from Eqs. (2) and (3) by a factor of 1.645 (i.e. confidence limit of 90%), and used them to assess the minimum limit of detection (LoD) for each displacement vector.

3.4 DEM assessment and elevation change analyses

The GCPs and CPs root mean square (RMS) errors from the bundle bloc orientation (Table 2) provide the overall sound quality of the UAV-SfM derived products. However, to further test the derived DEMs' elevation component, their accuracy was evaluated by comparing their modelled *z* coordinate to the measured *z* coordinate from ca 35 TGS points distributed on the rock glacier surface at the same date. This procedure also allowed to determine the possibility of systematic elevation errors (e.g. doming or dishing), which have been extensively reported for SfM derived datasets (James et al., 2017; Sanz-Ablanedo et al., 2020).

Elevation changes are obtained by computing DEMs of differences (DoD) from different periods, using the Geomorphic Change Detection (GCD) software (Wheaton et al., 2010). The errors on the DEMs are then propagated during the calculation of the DoD, and positive and negative elevation changes are obtained. A higher confidence interval (i.e. LoD at 95%) allowed distinguishing significant elevation changes between two DEMs (Clapuyt et al., 2017; Wheaton et al., 2010). Using the DoD analysis, mean thickness and volume changes were derived from the difference between the gain and loss of material. The DoD area of examination extends from the frontal position at ~2480 m asl to the upper section at 2615 m asl, which is the same distance as the velocity profiles in Figure 5.

4 Results

4.1 Validation of the UAV-derived velocities

Velocities obtained by in-situ GNSS surveys and UAV-derived data were analysed in detail for five consecutive periods from October 2016 to June 2019. Technical difficulties with the Leica AS10 GNSS base antenna impeded the measurement of all kinematic points during the last UAV survey in September 2019. Therefore, the comparison between GNSS and UAV-derived velocities was not completed for the June–September 2019 period. Using the exact initial position of 35 kinematic points, the whole range of UAV-derived velocities displayed a good agreement with the displacements of these points as measured by GNSS surveys (Fig 3). The correlation values for the consecutive periods were strong and significant, with R^2 values ranging between 0.98 and 0.99, indicating high reliability of the methodological approach. Individual outliers are mostly associated with kinematic points marked near the boulder edge. This is mainly because the cross-correlation tends to mismatch homologous points due to substantial changes in the geometry and lighting conditions. On the contrary, kinematics points installed near the boulder centre provide ideal cross-correlation targets for finding homologous points.

https://doi.org/10.5194/esurf-2021-8
Preprint. Discussion started: 23 February 2021

279

280 The individual LoDs calculated for each period displayed values ranging from 0.08 m (mostly for the 2017.06–2017.09 and
281 2018.06–2018.09 periods) up to 0.36 m (2016.10–2017.06 period) (Table 3). The largest errors are associated with the first
282 survey (October 2016). They are mainly due to a lower coregistration quality, which may derive from the strong shadows and
283 a thin sheet of snow existing during the UAV flight (Fig 4a). Still, values below LoD were concentrated at the northern and
284 southern margins (levees), where the rock glacier surface is virtually stable (Fig 4).

285 **4.2 Horizontal surface velocity fields**

286 Spatially distributed surface velocity fields of the Tsarmine rock glacier between October 2016 and September 2019 are shown
287 in Figure 4. Superficial velocities over 10 m yr^{-1} were measured during the last period analysed. The landform-wide velocity
288 fields depict lateral shearing margins between the highly active central part and the mostly stagnant northern and southern
289 levees (Fig 4). The velocities of both levees were below the LoD for most periods, but aside between September 2018 and
290 June 2019, where the southern levee displayed mean velocities of 0.21 m yr^{-1} (Fig 4e) towards the west. Between 2016 and
291 2019, the broad surface flow field displays a rather persistent direction towards the west in the upper and lower sections, with
292 mean values of 269° and 276°, respectively. A minor circular variance (i.e. how much vector directions deviate from the
293 directional mean) with values approaching zero for each study period also confirms a relatively low variability of this persistent
294 direction on the surface flow fields.

295

296 Remarkably, and during the entire period from 2016 to 2019, a sharp discontinuity expressed morphologically by developing
297 a scarp structure indicates the limit between two different kinematic units (indicated as “b” in Fig 5) with different temporal
298 behaviours. The mean values for the horizontal surface velocity fields (excluding the levees zones, see Fig 4) on the lower
299 portion of the rock glacier, that is the portion downstream of the scarp, ranged from 4.92 m yr^{-1} (2017.09–2018.06) to 8.74 m
300 yr^{-1} (2019.06–2019.09), whereas upslope they ranged from 2.83 m yr^{-1} (2017.09–2018.06) to 4.43 m yr^{-1} (2019.06–2019.09).
301 Moreover, between October 2016 and June 2018, a marked velocity decrease from 3.34 to 2.83 m yr^{-1} in the upper section
302 contrasts with a marginal decrease of velocities from 5.02 to 4.92 m yr^{-1} in the lower section (Table 4). On the other hand, the
303 mean surface displacements presented large seasonal differences between the snow cover (October to mid-June) and snow-
304 free (mid-June to late-September) periods. During the snow-free periods, displacement values share nearly a quarter of the
305 yearly component of the surface displacement (Table 4). It is worth to mention that these seasonal variations of rock glacier
306 displacements are in line with those observed by in-situ methods (Delaloye and Staub, 2016).

307 **4.3 High-resolution surface observations**

308 Aside from describing detailed surface velocity fields employing high-resolution orthomosaic pairs, the associated UAV-
309 derived datasets such as DEMs also allow describing some remarkable geomorphic changes on the rock glacier. Frontal line
310 changes between 2016 and 2019 are shown in Figure 6. The mean frontal positions relative to the October 2016 survey fluctuate

https://doi.org/10.5194/esurf-2021-8
Preprint. Discussion started: 23 February 2021

between -0.79 m (September 2017) and +2.42 m (June 2019). These changes reflect the oscillatory position of the rock glacier front at the time of each UAV survey acquisition. Despite the substantial surface displacements during the snow-free periods, the rock glacier front faces net erosion (frontal retreat). Likewise, during the snow cover period, the rock glacier front displays a net advance. This particular behaviour was also described between 2013 and 2016 by Kummert et al. (2018) using time series of in-situ webcam images.

The DoD analyses show a strongly heterogeneous elevation change pattern along the rock glacier (Fig 7). Aggregated over the surveyed area, the net elevation change between October 2016 and September 2019 is -0.21 ± 0.07 m. On the lower rock glacier section, large thickness changes varied between -7 to up to 7.5 m. However, almost non-significant changes are encountered in both levees sector. During the same period, the estimated volume gain is 12360 ± 1784 $m^{3,}$ whereas the volume loss is 22800 ± 2954 m^3 of material. The overall net volume change equates to -10526 ± 3451 m^3, indicating that wastage of material is considerably larger than the accumulation of material over the same surface. It is important to remark that the upper gully section, where the rock glacier is evacuating sediments from the terminus, is not included in the DoD analyses (for detailed characterization, the reader is referred to Kummert and Delaloye, 2018).

The 3-year development of the scarp structure across the entire width of the rock glacier (Fig 5), which was already existing at the time of the first survey, can be observed from the dynamic visualisation of the hillshade images at the video supplement (V1). At the time of the last UAV survey, the height of the scarp was reaching locally up to 10m (Fig 8). This dynamic visualisation also shows the passive transfer of material and an almost negligible rotational movement of boulders. Additionally, the video depicts the progressive enlargement in the southwestern margin (Fig 6b), which seats in direct contact with the stable southern levee, whereas in its northwestern portion, the rim has not expanded very significantly.

5 Discussions

5.1 UAV monitoring strategies

The close-range remote sensing monitoring approach based on repeated UAV surveys presents some benefits compared to other more classical remote sensing and in-situ techniques. First, as each segment of the remote sensing chain is controlled (Schott, 2007), from image acquisition, processing, and analysis, this approach is highly customisable to different monitoring periods (i.e. temporal resolution) and to the desired level of detail (i.e. spatial resolution). This is not trivial, as the users of classical photogrammetric surveys or satellite imagery cannot directly operate the platform, leaving their management into the hands of commercial or governmental agencies. Furthermore, this may hamper the optimal monitoring period and set prohibitive operational costs for the remote sensing strategy. Second, compared with TGS techniques, the time for data acquisition may be reduced when deploying UAV devices (provided that permanent GCPs are already established). On the field, a routine UAV flight operated from nearby takes less than 30 minutes to cover the rock glacier and its environs, whereas,

https://doi.org/10.5194/esurf-2021-8
Preprint. Discussion started: 23 February 2021

a regular TGS may take some hours (depending on the personnel's expertise) to measure the ensemble of kinematic points. With nearly optimal conditions during image acquisition, the LoD from UAV derived velocities is nearly as good as the one from GNSS measured velocities, but it can be substantially degraded during unfavourable conditions. Besides, the use of UAV helps increase personnel security by avoiding the terrestrial surveys on unstable sectors. This is especially the case in Tsarmine, where many boulders have become unstable and where the frontal area is always prone to rockfalls due to the strong rock glacier acceleration.

With operational fixed low costs and high spatial resolution, UAV surveys are well suited for studying medium-sized landforms (i.e. up to few hectares) at high monitoring rates (Rodriguez et al., 2020) but restricted to the snow-free period and the suitable environmental conditions for flying. For our study area, that means about four months a year (from mid-June to early October). Likewise, strong winds, fog, rain, ambient light, and suitable landing strips can further constrain or impede the operation of fixed-wing UAVs, particularly in high mountain terrain. National or international UAV regulations may pose additional restrictions or even prohibiting operating some UAV models on specific areas. In Switzerland, the Federal Office of Civil Aviation (FOCA) bans the operation of UAV devices on protected areas for water and migratory birds typically.

Regarding the specificities mentioned above, it is not surpassing that UAV monitoring approaches are gaining considerable momentum in geomorphological (Cook, 2017; Śledź et al., 2021) and cryospheric research (Gaffey and Bhardwaj, 2020). With this rapid growth of interest in UAV and SfM research, it can become clear that workflows and protocols need to be standardised. In an initial effort, Dall'Asta et al. (2017) employed fixed-wing UAV and GNSS devices to evaluate the surface displacements on a rock glacier located in the Aosta Valley, Italian Alps. Using SfM-derived datasets, such as orthophotos and DEMs, they evaluated the manual measurement of the rock glacier displacements and two automatic displacement methods based on the least-squares matching (LSM) and Semi-global matching (SGM) algorithms. In this particular case, they demonstrated that automatic methods outperformed the manual measurements of more than 1000 conjugate points by a trained operator. For a two-year period, they achieved similar R^2 values than our work but for a narrow range of displacements between 0–3 m. However, their work did not evaluate the stable ground outside the rock glacier, which may be a critical step for the detection of systematic bias during coregistration and the application of automatic displacements methods (Debella-Gilo and Kääb, 2011; Groh and Blöthe, 2019; Sorg et al., 2015).

More recently, the work carried out by Fey and Krainer (2020) also employed UAV and GNSS data to derive flow velocities on the Lazaun rock glacier, which is located in the Schnals Valley, Italian Alps. Nonetheless, because some of the work was entrusted to different external companies (i.e. outsourced), neither the UAV nor the GNSS processing steps could be described in their study. Therefore, intrinsic data processing quality for each survey was not available (like our Table 2). From our side, we performed all the data collection, essential processing steps, and analyses of our datasets. Furthermore, they employed the marked kinematic points as GCPs for the UAV acquisition (between 42 and 71 points), whereas we used such points only for

https://doi.org/10.5194/esurf-2021-8
Preprint. Discussion started: 23 February 2021

the UAV-derived velocities validation (Fig. 3). In this fashion, we want to emphasise that our kinematic points are explicitly used to provide independent accuracy examinations. Besides, such a large number of GCPs will be impractical for some rock glaciers, where terrain constraints such as unstable ground and accessibility will compromise the safety of the monitoring efforts.

5.2 UAV and TGS frameworks

As we indicated in our methodology using sequential orthomosaics, we consider the calculation of UAV-derived velocities using a fixed grid system (video supplement V2) through which the rock glacier surface flows (i.e. Eulerian specification of the surface flow fields). It should be stressed that during the validation step, we actually employed the initial coordinates of the kinematic points that corresponded to each UAV survey acquisition (Sec. 3.3). This procedure was necessary for comparing the UAV-derived and GNSS measured velocities on the same position (i.e. x and y coordinates CH1903+ LV95). By contrast, the TGS alone provides velocities values using a moving net of marked boulders (video supplement V3) as it moves along the rock glacier surface (i.e. Lagrangian specification of the surface flow fields). In the case of steady rock glacier velocities, or over short-term periods, the Lagrangian (TGS) and Eulerian (UAV-derived) systems are expected to provide comparable results. However, the values provided by each system might diverge during large displacements. This can be illustrated by the surveyed boulders that were initially labelled to belong to either the rooting or central zones, and which are currently at (or heading to) the rock glacier upper central or frontal zones, respectively (PERMOS, 2019b). Thus, such measurements are not representing the original rock glacier zonification.

5.3 Recent kinematic behaviour

Overall, the rock glacier has displayed a nearly continuous acceleration and the ongoing development of a scarp feature during the survey period. This landform does not fit the conveyor belt advancing model (Kääb and Reichmuth, 2005) and corresponds to the less frequent rock glacier configuration with an advancing and eroding terminus (rock glacier type B sensu Kummert et al., 2018). At the front, active erosion processes have compensated the average frontal displacement of 18 m between October 2016 and September 2019. Besides, sediments are efficiently evacuated at the front of the rock glacier through a steep gully (Kummert and Delaloye, 2018), and therefore the rock glacier terminus is oscillating from season to season (Fig. 6). During most of the snow cover periods, the freezing of the active layer explains the net frontal advances identified in mid-June. This freezing leads to increasing ice content and cementing rock particles, and consequently, reducing the frontal erosion rates during the cold periods (Kummert et al., 2018). Contrarily, the thawing of the active layer and the freshly exposed permafrost ground during the snow-free periods generates increased erosion rates and net frontal retreats (Fig 6). The high frontal velocities and the enhancement of the transversal scarp feature indicate a destabilisation phase (Marcer et al., 2019). However, a potential collapse of the landform is not expected, even if the high velocities persist, due to two main reasons: (1) the net surface elevation gain observed along the rock glacier front which is leading toward to a concave profile (Fig 7) and; (2) the incremental sediment transfer rates concomitant with the rock glacier acceleration (Kummert and Delaloye, 2018).

https://doi.org/10.5194/esurf-2021-8
Preprint. Discussion started: 23 February 2021

409

410 The onset of the scarp feature predates the monitoring period using UAV surveys, and the use of sparse kinematic points from
411 previous TGS can help reveal the initial conditions of this feature. As can be seen from Figure 9, two kinematic points
412 representing the lower (15) and upper (33) sections are plotted between 2004 and 2020. They show a clear divergence in their
413 surface velocities from 2012 onwards. The ongoing change in rock glacier dynamics has gradually produced a situation where
414 the active layer and the upper permafrost core in particular (mostly coarse-grained rocks and boulders with interstitial ice, see
415 Figure 8b) are no capable to deform fast enough to compensate the stress-induced failures. Contrarily, around the position of
416 the shear horizon (mostly a finer-grained sediment frozen layer) plastic deformation can still occur (Moore, 2014), and
417 therefore, could prevent the superficial failure to split the rock glacier into two independent sections brutally. This particular
418 behaviour has been previously observed at Petit-Velan (Delaloye and Morard, 2011) and Grosse Grabe (Delaloye et al., 2013)
419 rock glaciers, which are also situated in the Western Swiss Alps.

420

421 In a recent example, Strozzi et al. (2020) presented results of satellite radar interferometry (InSAR) to monitor the kinematics
422 of Tsarmine rock glacier between 2009 and 2020. Using early Cosmo-SkyMed and recent Sentinel-1 radar imagery, they were
423 able to display the occurrence of a substantial seasonal variability of the uppermost section of the rock glacier, which has been
424 mostly in line with the one observed by the permanent GNSS station on its terminal part (see Fig. 1). However, decorrelation
425 problems between 2016 and 2019 caused by rapid displacements and the relatively small rock glacier surface area inhibited
426 the capture of the spatial variability of the surface velocities. Hence, Strozzi et al. (2020) presented the results that could not
427 detect the significant velocity variations along the entire length of the central profile (Fig 5) between October 2016 and
428 September 2019 and are restricted to the uppermost slower portion. Regarding the recent popularity and extensive analysis of
429 rock glaciers using InSAR (e.g. Bertone et al., 2019; Villarroel et al., 2018), precautions on the interpretation of landform
430 kinematic should be taken when small and rapid features with heterogeneous kinematic values are investigated. The quality of
431 the high-resolution UAV-derived datasets leads us to stress that regular and spatially distributed surface velocity measurements
432 based on the proposed uncertainty analysis would permit landform-wide kinematics to be better monitored.

433 **6 Conclusions**

434 The customised UAV data acquisition and the subsequent robust data processing workflow delivered spatially distributed rock
435 glacier kinematics for the 2016–2019 period. Between June and September 2019, superficial velocities in excess of 10 m yr^{-1}
436 were measured on the lower part of the rock glacier. The DoD analysis highlighted large elevation changes concentrated on
437 the lower rock glacier section. The applied methodology of the UAV campaigns has provided valuable data that is in good
438 agreement with those obtained by TGS using GNSS equipment. Our results provide strong support for the use of UAV and
439 automatic image matching for the enhanced analysis of the spatio-temporal rock glacier kinematic, as well as going beyond
440 traditional survey methods.

https://doi.org/10.5194/esurf-2021-8
Preprint. Discussion started: 23 February 2021

441

442 Furthermore, thanks to the very high resolution and spatial coverage, the scarp development and the abrupt velocity differences
443 between the lower and upper rock glacier sections could be documented. During similar periods, these characteristics have
444 been described by neither TGS surveys nor other remote sensing data such as InSAR. In this regard, we stress the importance
445 of timely and high-resolution surface observations to decipher landform dynamics and to improve our understating of rock
446 glacier behaviour during destabilisation phases.

447

448 New and adaptable monitoring techniques are further needed to monitor rock glaciers and other mountain landforms that are
449 reacting quickly to environmental changes. This work detailed the use of UAV surveys and SfM techniques to monitor rapid
450 kinematic changes on an active rock glacier with enhanced temporal and spatial details. Hence, the monitoring of rock glacier
451 kinematics with in-situ techniques (i.e. TGS and TLS) can be complemented with regular UAVs surveys over selected rock
452 glaciers. Where rock glaciers are becoming highly unstable and dangerous, repeated UAV surveys are an adequate tool to
453 monitor such landforms.

454

455 In Tsarmine, additional work should address the influence of the rock glacier acceleration on the scarp development and
456 evolution to better understand the rheology of destabilised rock glaciers. This includes modelling approaches and quantifying
457 historical velocities by reanalysis of archival aerial photographs available for this rock glacier. Moreover, further developments
458 on rock glacier studies should target the assessment of volumetric changes and geodetic mass balance (see Kellerer-Pirklbauer
459 and Kaufmann, 2018) at very high resolution using the high-quality UAV-derived data such as DEMs or point clouds.

460

461 **Data availability.** The corresponding author upon request can provide additional data for this study. The complete series of
462 interactive 3D models from Tsarmine rock glacier is available at https://sketchfab.com/UNIL-IDYST/collections/tsarmine-
463 rock-glacier. The kinematic data from Tsarmine rock glacier is available from the PERMOS office upon request. The reference
464 website link is http://www.permos.ch/data.html.

465

466 **Video supplement.** Videos are the animation of the sequential hillshaded DEM and orthomosaics of the Tsarmine rock glacier
467 between 2016 and 2019. The V1 corresponds to the hillshade animation where the ongoing scarp development can be seen.
468 V2 and V3 are the orthomosaics animations illustrating the difference between TGS and UAV frameworks.

469

470 **Author contributions.** SV performed data acquisition, processing, and analyses, wrote the initial version of the manuscript
471 and designed all the figures under the rigorous supervision of CL. RD assisted with GNSS data acquisition and critical feedback
472 from the results.

473

474 **Competing interests.** The authors declare that they have no conflict of interest.

https://doi.org/10.5194/esurf-2021-8
Preprint. Discussion started: 23 February 2021

Acknowledgements. Our gratitude goes to the Tsarmine field team from the Universities of Lausanne and Fribourg, and Sébastien Rüttimann, for helping with the earlier UAV. We also acknowledge the opportunistic employment of the permanent GCPs installed during a previous study by Umberto Morra di Cella.

References

Arenson, L. U., Hoelzle, M. and Springman, S.: Borehole deformation measurements and internal structure of some rock glaciers in Switzerland, Permafr. Periglac. Process., 13(2), 117–135, doi:10.1002/ppp.414, 2002.

Barsch, D.: Rockglaciers: indicators for the present and former geoecology in high mountain environments, Springer-Verlag, Berlin., 1996.

Benassi, F., Dall'Asta, E., Diotri, F., Forlani, G., Morra di Cella, U., Roncella, R. and Santise, M.: Testing Accuracy and Repeatability of UAV Blocks Oriented with GNSS-Supported Aerial Triangulation, Remote Sens., 9(2), 172, doi:10.3390/rs9020172, 2017.

Benoit, L., Gourdon, A., Vallat, R., Irarrazaval, I., Gravey, M., Lehmann, B., Prasicek, G., Gräff, D., Herman, F. and Mariethoz, G.: A high-resolution image time series of the Gorner Glacier - Swiss Alps - derived from repeated unmanned aerial vehicle surveys, Earth Syst. Sci. Data, 11(2), 579–588, doi:10.5194/essd-11-579-2019, 2019.

Berthling, I., Etzelmüller, B., Eiken, T. and Sollid, J. L.: Rock glaciers on Prins Karls Forland, Svalbard. I: internal structure, flow velocity and morphology, Permafr. Periglac. Process., 9(2), 135–145, doi:10.1002/(SICI)1099-1530(199804/06)9:2<135::AID-PPP284>3.0.CO;2-R, 1998.

Bertone, A., Zucca, F., Marin, C., Notarnicola, C., Cuozzo, G., Krainer, K., Mair, V., Riccardi, P., Callegari, M. and Seppi, R.: An unsupervised method to detect rock glacier activity by using Sentinel-1 SAR interferometric coherence: A regional-scale study in the Eastern European Alps, Remote Sens., 11(14), doi:10.3390/rs11141711, 2019.

Blöthe, J. H., Halla, C., Schwalbe, E., Bottegal, E., Trombotto Liaudat, D. and Schrott, L.: Surface velocity fields of active rock glaciers and ice-debris complexes in the Central Andes of Argentina, Earth Surf. Process. Landforms, esp.5042, doi:10.1002/esp.5042, 2020.

Bodin, X., Thibert, E., Fabre, D., Ribolini, A., Schoeneich, P., Francou, B., Reynaud, L. and Fort, M.: Two decades of responses (1986-2006) to climate by the laurichard rock glacier, French alps, Permafr. Periglac. Process., 20(4), 331–344, doi:10.1002/ppp.665, 2009.

Bodin, X., Krysiecki, J. M., Schoeneich, P., Le Roux, O., Lorier, L., Echelard, T., Peyron, M. and Walpersdorf, A.: The 2006 Collapse of the Bérard Rock Glacier (Southern French Alps), Permafr. Periglac. Process., 28(1), 209–223, doi:10.1002/ppp.1887, 2017.

Bollmann, E., Girstmair, A., Mitterer, S., Krainer, K., Sailer, R. and Stötter, J.: A Rock Glacier Activity Index Based on Rock Glacier Thickness Changes and Displacement Rates Derived From Airborne Laser Scanning, Permafr. Periglac. Process.,

26(4), 347–359, doi:10.1002/ppp.1852, 2015.

Buchli, T., Kos, A., Limpach, P., Merz, K., Zhou, X. and Springman, S. M.: Kinematic investigations on the Furggwanghorn Rock Glacier, Switzerland, Permafr. Periglac. Process., 29(1), 3–20, doi:10.1002/ppp.1968, 2018.

Carbonneau, P. E. and Dietrich, J. T.: Cost-effective non-metric photogrammetry from consumer-grade sUAS: implications for direct georeferencing of structure from motion photogrammetry, Earth Surf. Process. Landforms, 42(3), 473–486, doi:10.1002/esp.4012, 2017.

Carrivick, J. L., Smith, M. W. and Quincey, D. J.: Structure from Motion in the Geosciences, John Wiley & Sons, Ltd, Chichester, UK., 2016.

Cicoira, A., Beutel, J., Faillettaz, J. and Vieli, A.: Water controls the seasonal rhythm of rock glacier flow, Earth Planet. Sci. Lett., 528, 115844, doi:10.1016/j.epsl.2019.115844, 2019.

Cicoira, A., Marcer, M., Gärtner-Roer, I., Bodin, X., Arenson, L. U. and Vieli, A.: A general theory of rock glacier creep based on in-situ and remote sensing observations, Permafr. Periglac. Process., ppp.2090, doi:10.1002/ppp.2090, 2020.

Clapuyt, F., Vanacker, V., Schlunegger, F. and Van Oost, K.: Unravelling earth flow dynamics with 3-D time series derived from UAV-SfM models, Earth Surf. Dyn., 5(4), 791–806, doi:10.5194/esurf-5-791-2017, 2017.

Clifford, S. M., George, J. A. and Stoker, C. R.: Introduction to the special section: Geophysical detection of subsurface water on Mars, J. Geophys. Res., 108(E4), 8020, doi:10.1029/2003JE002068, 2003.

Cook, K. L.: An evaluation of the effectiveness of low-cost UAVs and structure from motion for geomorphic change detection, Geomorphology, 278, 195–208, doi:10.1016/j.geomorph.2016.11.009, 2017.

Dall'Asta, E., Forlani, G., Roncella, R., Santise, M., Diotri, F. and Morra di Cella, U.: Unmanned Aerial Systems and DSM matching for rock glacier monitoring, ISPRS J. Photogramm. Remote Sens., 127, 102–114, doi:10.1016/j.isprsjprs.2016.10.003, 2017.

Debella-Gilo, M. and Kääb, A.: Sub-pixel precision image matching for measuring surface displacements on mass movements using normalized cross-correlation, Remote Sens. Environ., 115(1), 130–142, doi:10.1016/j.rse.2010.08.012, 2011.

Delaloye, R. and Morard, S.: Le glacier rocheux déstabilisé du Petit-Vélan (Val d'Entremont, Valais): morphologie de surface, vitesses de déplacement et structure interne, La géomorphologie Alp. entre patimoine contrainte. Actes du Colloq. la Société Suisse Géomorphologie, 3-5 Sept. 2009, Olivone (Géovisions n° 36). Inst. géographie, Univ. Lausanne., 197–210, 2011.

Delaloye, R. and Staub, B.: Seasonal variations of rock glacier creep: Time series observations from the Western Swiss Alps, in XI. International Conference On Permafrost – Book of Abstracts, edited by F. Günther and A. Morgenstern, pp. 20–24, Potsdam., 2016.

Delaloye, R., Avian, M., Bodin, X., Hausmann, H., Ikeda, A., Kääb, A., Kellerer-Pirklbauer, A., Krainer, K. and Lambiel, C.: Recent interannual variations of rockglacier creep in the European Alps, in Proceedings of the 9th International Conference on Permafrost, pp. 1–6, Fairbanks., 2008.

Delaloye, R., Lambiel, C. and Gärtner-Roer, I.: Overview of rock glacier kinematics research in the Swiss Alps: seasonal rhythm, interannual variations and trends over several decades, Geogr. Helv., 65, 135–145, doi:10.5194/gh-65-135-2010,

2010.

Delaloye, R., Morard, S., Barboux, C., Abbet, D., Gruber, V., Riedo, M. and Gachet, S.: Rapidly moving rock glaciers in Mattertal, Jahrestagung der Schweizerischen Geomorphol. Gesellschaft, (i), 21–31, 2013.

Deline, P., Gruber, S., Delaloye, R., Fischer, L., Geertsema, M., Giardino, M., Hasler, A., Kirkbride, M. P., Krautblatter, M., Magnin, F., McColl, S., Ravanel, L. and Schoeneich, P.: Ice Loss and Slope Stability in High-Mountain Regions, in Snow and Ice-Related Hazards, Risks and Disasters, pp. 521–561, Elsevier., 2015.

Deluigi, N., Lambiel, C. and Kanevski, M.: Data-driven mapping of the potential mountain permafrost distribution, Sci. Total Environ., 590–591, 370–380, doi:10.1016/j.scitotenv.2017.02.041, 2017.

Eichel, J., Draebing, D., Kattenborn, T., Senn, J. A., Klingbeil, L., Wieland, M. and Heinz, E.: Unmanned aerial vehicle-based mapping of turf-banked solifluction lobe movement and its relation to material, geomorphometric, thermal and vegetation properties, Permafr. Periglac. Process., 31(1), 97–109, doi:10.1002/ppp.2036, 2020.

Eriksen, H. Ø., Rouyet, L., Lauknes, T. R., Berthling, I., Isaksen, K., Hindberg, H., Larsen, Y. and Corner, G. D.: Recent Acceleration of a Rock Glacier Complex, Ádjet, Norway, Documented by 62 Years of Remote Sensing Observations, Geophys. Res. Lett., 45(16), 8314–8323, doi:10.1029/2018GL077605, 2018.

Fey, C. and Krainer, K.: Analyses of UAV and GNSS based flow velocity variations of the rock glacier Lazaun (Ötztal Alps, South Tyrol, Italy), Geomorphology, 107261, doi:10.1016/j.geomorph.2020.107261, 2020.

Forlani, G., Dall'Asta, E., Diotri, F., di Cella, U. M., Roncella, R. and Santise, M.: Quality assessment of DSMs produced from UAV flights georeferenced with on-board RTK positioning, Remote Sens., 10(2), doi:10.3390/rs10020311, 2018.

Francou, B. and Reynaud, L.: 10 year surficial velocities on a rock glacier (Laurichard, French Alps), Permafr. Periglac. Process., 3(3), 209–213, doi:10.1002/ppp.3430030306, 1992.

Frehner, M., Ling, A. H. M. and Gärtner-Roer, I.: Furrow-and-ridge morphology on rockglaciers explained by gravity-driven buckle folding: A case study from the murtèl rockglacier (Switzerland), Permafr. Periglac. Process., 26(1), 57–66, doi:10.1002/ppp.1831, 2015.

Fugazza, D., Scaioni, M., Corti, M., D'Agata, C., Azzoni, R. S., Cernuschi, M., Smiraglia, C. and Diolaiuti, G. A.: Combination of UAV and terrestrial photogrammetry to assess rapid glacier evolution and map glacier hazards, Nat. Hazards Earth Syst. Sci., 18(4), 1055–1071, doi:10.5194/nhess-18-1055-2018, 2018.

Gaffey, C. and Bhardwaj, A.: Applications of Unmanned Aerial Vehicles in Cryosphere: Latest Advances and Prospects, Remote Sens., 12(6), 948, doi:10.3390/rs12060948, 2020.

Groh, T. and Blöthe, J. H.: Rock Glacier Kinematics in the Kaunertal, Ötztal Alps, Austria, Geosciences, 9(9), 373, doi:10.3390/geosciences9090373, 2019.

Haeberli, W., Hallet, B., Arenson, L. U., Elconin, R., Humlum, O., Kääb, A., Kaufmann, V., Ladanyi, B., Matsuoka, N., Springman, S. M. and Mühll, D. V.: Permafrost creep and rock glacier dynamics, Permafr. Periglac. Process., 17(3), 189–214, doi:10.1002/ppp.561, 2006.

Hartl, L., Fischer, A., Stocker-Waldhuber, M. and Abermann, J.: Recent speed-up of an alpine rock glacier: An updated

https://doi.org/10.5194/esurf-2021-8
Preprint. Discussion started: 23 February 2021

575 chronology of the kinematics of outer hochebenkar rock glacier based on geodetic measurements, Geogr. Ann. Ser. A, Phys.
576 Geogr., 98(2), 129–141, doi:10.1111/geoa.12127, 2016.
577 Heid, T. and Kääb, A.: Evaluation of existing image matching methods for deriving glacier surface displacements globally
578 from optical satellite imagery, Remote Sens. Environ., 118, 339–355, doi:10.1016/j.rse.2011.11.024, 2012.
579 Hendrickx, H., Vivero, S., De Cock, L., De Wit, B., De Maeyer, P., Lambiel, C., Delaloye, R., Nyssen, J. and Frankl, A.: The
580 reproducibility of SfM algorithms to produce detailed Digital Surface Models: the example of PhotoScan applied to a high-
581 alpine rock glacier, Remote Sens. Lett., 10(1), 11–20, doi:10.1080/2150704X.2018.1519641, 2019.
582 Hendrickx, H., De Sloover, L., Stal, C., Delaloye, R., Nyssen, J. and Frankl, A.: Talus slope geomorphology investigated at
583 multiple time scales from high-resolution topographic surveys and historical aerial photographs (Sanetsch Pass, Switzerland),
584 Earth Surf. Process. Landforms, doi:10.1002/esp.4989, 2020.
585 Hubbard, B., Souness, C. and Brough, S.: Glacier-like forms on Mars, Cryosphere, 8(6), 2047–2061, doi:10.5194/tc-8-2047-
586 2014, 2014.
587 Ikeda, A. and Matsuoka, N.: Pebbly versus bouldery rock glaciers: Morphology, structure and processes, Geomorphology,
588 73(3–4), 279–296, doi:10.1016/j.geomorph.2005.07.015, 2006.
589 Ikeda, A., Matsuoka, N. and Kääb, A.: Fast deformation of perennially frozen debris in a warm rock glacier in the Swiss Alps:
590 An effect of liquid water, J. Geophys. Res. Earth Surf., 113(1), 1–12, doi:10.1029/2007JF000859, 2008.
591 James, M. R. and Robson, S.: Straightforward reconstruction of 3D surfaces and topography with a camera: Accuracy and
592 geoscience application, J. Geophys. Res. Earth Surf., 117(3), 1–17, doi:10.1029/2011JF002289, 2012.
593 James, M. R., Robson, S. and Smith, M. W.: 3-D uncertainty-based topographic change detection with structure-from-motion
594 photogrammetry: precision maps for ground control and directly georeferenced surveys, Earth Surf. Process. Landforms,
595 42(12), 1769–1788, doi:10.1002/esp.4125, 2017.
596 Janke, J. R., Regmi, N. R., Giardino, J. R. and Vitek, J. D.: Rock Glaciers, in Treatise on Geomorphology, vol. 8, pp. 238–
597 273, Elsevier., 2013.
598 Jones, D. B., Harrison, S., Anderson, K. and Betts, R. A.: Mountain rock glaciers contain globally significant water stores, Sci.
599 Rep., 8(1), 1–10, doi:10.1038/s41598-018-21244-w, 2018.
600 Kääb, A.: Remote sensing of mountain glaciers and permafrost creep, Geographisches Institut der Univ. Zurich., 2005.
601 Kääb, A. and Reichmuth, T.: Advance mechanisms of rock glaciers, Permafr. Periglac. Process., 16(2), 187–193,
602 doi:10.1002/ppp.507, 2005.
603 Kääb, A. and Vollmer, M.: Surface Geometry, Thickness Changes and Flow Fields on Creeping Mountain Permafrost:
604 Automatic Extraction by Digital Image Analysis, Permafr. Periglac. Process., 11(4), 315–326, doi:10.1002/1099-
605 1530(200012)11:4<315::AID-PPP365>3.0.CO;2-J, 2000.
606 Kääb, A., Haeberli, W. and Gudmundsson, G. H.: Analysing the creep of mountain permafrost using high precision aerial
607 photogrammetry: 25 years of monitoring Gruben rock glacier, Swiss Alps, Permafr. Periglac. Process., 8(4), 409–426,
608 doi:10.1002/(SICI)1099-1530(199710/12)8:4<409::AID-PPP267>3.0.CO;2-C, 1997.

https://doi.org/10.5194/esurf-2021-8
Preprint. Discussion started: 23 February 2021

609 Kääb, A., Frauenfelder, R. and Roer, I.: On the response of rockglacier creep to surface temperature increase, Glob. Planet.
610 Change, 56, 172–187, 2007.
611 Kaufmann, V.: 20 years of geodetic monitoring of Dösen rock glacier (Ankogel group, Austria): A short review [20 Jahre
612 geodätischer Beobachtung am Dösener Blockgletscher (Ankogelgruppe, Österreich): Ein kurzer Überblick], Joannea - Geol.
613 und Palaontologie, 12, 37–44 [online] Available from: https://www.scopus.com/inward/record.uri?eid=2-s2.0-
614 85007448664&partnerID=40&md5=bc3087cd8170f8b134d0a85dac23d6f6, 2016.
615 Kellerer-Pirklbauer, A. and Kaufmann, V.: Deglaciation and its impact on permafrost and rock glacier evolution: New insight
616 from two adjacent cirques in Austria, Sci. Total Environ., 621, 1397–1414, doi:10.1016/j.scitotenv.2017.10.087, 2018.
617 Kellerer-Pirklbauer, A., Wangensteen, B., Farbrot, H. and Etzelmüller, B.: Relative surface age-dating of rock glacier systems
618 near Hólar in Hjaltadalur, northern Iceland, J. Quat. Sci., 23(2), 137–151, doi:10.1002/jqs, 2008.
619 Kellerer-Pirklbauer, A., Lieb, G. K. and Kaufmann, V.: The Dösen rock glacier in Central Austria: A key site for
620 multidisciplinary long-term rock glacier monitoring in the Eastern Alps, Austrian J. Earth Sci., 110(2),
621 doi:10.17738/ajes.2017.0013, 2017.
622 Kellerer-Pirklbauer, A., Delaloye, R., Lambiel, C., Gärtner-Roer, I., Kaufmann, V., Scapozza, C., Krainer, K., Staub, B.,
623 Thibert, E., Bodin, X., Fischer, A., Hartl, L., Morra Di Cella, U., Mair, V., Marcer, M. and Schoeneich, P.: Interannual
624 variability of rock glacier flow velocities in the European Alps, in Proceedings of the 5th European Conference on Permafrost
625 (EUCOP5-2018), pp. 396–397, Chamonix, France., 2018.
626 Koning, D. M. and Smith, D. J.: Movement of King's Throne rock glacier, Mount Rae Area, Canadian Rocky Mountains,
627 Permafr. Periglac. Process., 10(2), 151–162, doi:10.1002/(SICI)1099-1530(199904/06)10:2<151::AID-PPP312>3.0.CO;2-R,
628 1999.
629 Konrad, S. K., Humphrey, N. F., Steig, E. J., Clark, D. H., Potter, N. and Pfeffer, W. T.: Rock glacier dynamics and
630 paleoclimatic implications, Geology, 27(12), 1131, doi:10.1130/0091-7613(1999)027<1131:RGDAPI>2.3.CO;2, 1999.
631 Krainer, K., Bressan, D., Dietre, B., Haas, J. N., Hajdas, I., Lang, K., Mair, V., Nickus, U., Reidl, D., Thies, H. and Tonidandel,
632 D.: A 10,300-year-old permafrost core from the active rock glacier Lazaun, southern Ötztal Alps (South Tyrol, northern Italy),
633 Quat. Res. (United States), 83(2), 324–335, doi:10.1016/j.yqres.2014.12.005, 2015.
634 Kummert, M. and Delaloye, R.: Mapping and quantifying sediment transfer between the front of rapidly moving rock glaciers
635 and torrential gullies, Geomorphology, 309, 60–76, doi:10.1016/j.geomorph.2018.02.021, 2018.
636 Kummert, M., Delaloye, R. and Braillard, L.: Erosion and sediment transfer processes at the front of rapidly moving rock
637 glaciers: Systematic observations with automatic cameras in the western Swiss Alps, Permafr. Periglac. Process., 29(1), 21–
638 33, doi:10.1002/ppp.1960, 2018.
639 Lambiel, C.: Le pergélisol dans les terrains sédimentaires à forte déclivité: distribution, régime thermique et instabilités,
640 Université de Lausanne. [online] Available from: https://serval.unil.ch/notice/serval:BIB_R_6234 (Accessed 20 August 2020),
641 2006.
642 Lambiel, C.: Glacial and Periglacial Landscapes in the Hérens Valley, in World Geomorphological Landscapes, edited by E.

643 Reynard, pp. 263–275, Springer., 2021.
644 Lambiel, C. and Delaloye, R.: Contribution of real-time kinematic GPS in the study of creeping mountain permafrost:
645 Examples from the Western Swiss Alps, Permafr. Periglac. Process., 15(3), 229–241, doi:10.1002/ppp.496, 2004.
646 Lowe, D. G.: Distinctive Image Features from Scale-Invariant Keypoints, Int. J. Comput. Vis., 60(2), 91–110,
647 doi:10.1023/B:VISI.0000029664.99615.94, 2004.
648 Lucieer, a., Jong, S. M. D. and Turner, D.: Mapping landslide displacements using Structure from Motion (SfM) and image
649 correlation of multi-temporal UAV photography, Prog. Phys. Geogr., 38, 97–116, doi:10.1177/0309133313515293, 2013.
650 Marcer, M., Serrano, C., Brenning, A., Bodin, X., Goetz, J. and Schoeneich, P.: Evaluating the destabilization susceptibility
651 of active rock glaciers in the French Alps, Cryosph., 13(1), 141–155, doi:10.5194/tc-13-141-2019, 2019.
652 Marcer, M., Ringsø Nielsen, S., Ribeyre, C., Kummert, M., Duvillard, P. A., Schoeneich, P., Bodin, X. and Genuite, K.:
653 Investigating the slope failures at the Lou rock glacier front, French Alps, Permafr. Periglac. Process., 31(1), 15–30,
654 doi:10.1002/ppp.2035, 2020.
655 Messerli, B. and Zurbuchen, M.: Block-gletscher im Weissmies und Aletsch und ihre photogrammetrische Kartierung., Die
656 Alpen, 3, 139–152 [online] Available from: https://ci.nii.ac.jp/naid/20001586467/ (Accessed 13 May 2020), 1968.
657 Micheletti, N., Lambiel, C. and Lane, S. N.: Investigating decadal-scale geomorphic dynamics in an alpine mountain setting,
658 J. Geophys. Res. Earth Surf., 120(10), 2155–2175, doi:10.1002/2015JF003656, 2015.
659 Micheletti, N., Tonini, M. and Lane, S. N.: Geomorphological activity at a rock glacier front detected with a 3D density-based
660 clustering algorithm, Geomorphology, 278, 287–297, doi:10.1016/j.geomorph.2016.11.016, 2016.
661 Moore, P. L.: Deformation of debris-ice mixtures, Rev. Geophys., 52(3), 435–467, doi:10.1002/2014RG000453, 2014.
662 Müller, J., Vieli, A. and Gärtner-Roer, I.: Rock glaciers on the run - Understanding rock glacier landform evolution and recent
663 changes from numerical flow modeling, Cryosphere, 10(6), 2865–2886, doi:10.5194/tc-10-2865-2016, 2016.
664 Necsoiu, M., Onaca, A., Wigginton, S. and Urdea, P.: Rock glacier dynamics in Southern Carpathian Mountains from high-
665 resolution optical and multi-temporal SAR satellite imagery, Remote Sens. Environ., 177, 21–36,
666 doi:10.1016/j.rse.2016.02.025, 2016.
667 Nex, F. and Remondino, F.: UAV for 3D mapping applications: A review, Appl. Geomatics, 6(1), 1–15, doi:10.1007/s12518-
668 013-0120-x, 2014.
669 PERMOS: Permafrost in Switzerland 2008/2009 and 2009/2010, edited by J. Nötzli, Cryospheric Commission of the Swiss
670 Academy of Sciences., 2013.
671 PERMOS: Permafrost in Switzerland 2014/2015 to 2017/2018, edited by J. Nötzli, C. Pellet, and B. Staub, Cryospheric
672 Commission of the Swiss Academy of Sciences., 2019a.
673 PERMOS: PERMOS Database, Swiss Permafrost Monitoring Network, Fribourg and Davos, Switzerland, ,
674 doi:DOI:10.13093/permos-2019-01, 2019b.
675 Redpath, T. A. N., Sirguey, P., Fitzsimons, S. J. and Kääb, A.: Accuracy assessment for mapping glacier flow velocity and
676 detecting flow dynamics from ASTER satellite imagery: Tasman Glacier, New Zealand, Remote Sens. Environ., 133, 90–101,

677 doi:10.1016/j.rse.2013.02.008, 2013.
678 Rignot, E., Hallet, B. and Fountain, A. G.: Rock glacier surface motion in Beacon Valley, Antarctica, from synthetic-aperture
679 radar interferometry, Geophys. Res. Lett., 29(12), 48–51, doi:10.1029/2001GL013494, 2002.
680 Rodriguez, J., Macciotta, R., Hendry, M. T., Roustaei, M., Gräpel, C. and Skirrow, R.: UAVs for monitoring, investigation,
681 and mitigation design of a rock slope with multiple failure mechanisms—a case study, Landslides, (April),
682 doi:10.1007/s10346-020-01416-4, 2020.
683 Roer, I., Kääb, A. and Dikau, R.: Rockglacier acceleration in the Turtmann valley (Swiss Alps): Probable controls, Nor. Geogr.
684 Tidsskr. - Nor. J. Geogr., 59(February 2015), 157–163, doi:10.1080/00291950510020655, 2005.
685 Roer, I., Haeberli, W., Avian, M., Kaufmann, V., Delaloye, R., Lambiel, C. and Kääb, A.: Observations and considerations on
686 destabilizing active rock glaciers in the European Alps, in Proceedings of the 9th International Conference on Permafrost, pp.
687 1505–1510, Fairbanks., 2008.
688 Rossini, M., Di Mauro, B., Garzonio, R., Baccolo, G., Cavallini, G., Mattavelli, M., De Amicis, M. and Colombo, R.: Rapid
689 melting dynamics of an alpine glacier with repeated UAV photogrammetry, Geomorphology, 304, 159–172,
690 doi:10.1016/j.geomorph.2017.12.039, 2018.
691 Ryan, J. C., Hubbard, a. L., Box, J. E., Todd, J., Christoffersen, P., Carr, J. R., Holt, T. O. and Snooke, N.: UAV
692 photogrammetry and structure from motion to assess calving dynamics at Store Glacier, a large outlet draining the Greenland
693 ice sheet, Cryosph., 9, 1–11, doi:10.5194/tc-9-1-2015, 2015.
694 Sanz-Ablanedo, E., Chandler, J. H., Ballesteros-Pérez, P. and Rodríguez-Pérez, J. R.: Reducing systematic dome errors in
695 digital elevation models through better UAV flight design, Earth Surf. Process. Landforms, 2147(May), 2134–2147,
696 doi:10.1002/esp.4871, 2020.
697 Savšek-Safic, S., Ambrožič, T., Stopar, B. and Turk, G.: Determination of point displacements in the geodetic network, J.
698 Surv. Eng., 132(2), 58–63, doi:10.1061/(ASCE)0733-9453(2006)132:2(58), 2006.
699 Schneider, B. and Schneider, H.: Zur 60jährigen Messreihe der kurzfristigen Geschwindigkeitsschwankungen am
700 Blockgletscher im Äusseren Hochebenkar, Ötztaler Alpen, Tirol., Zeitschrift für Gletscherk. u. Glazialg, 37(1), 1–33, 2001.
701 Schott, J. R.: Remote Sensing: The Image Chain Approach., 2007.
702 Scotti, R., Crosta, G. B. and Villa, A.: Destabilisation of Creeping Permafrost: The Plator Rock Glacier Case Study (Central
703 Italian Alps), Permafr. Periglac. Process., 28(1), 224–236, doi:10.1002/ppp.1917, 2017.
704 Śledź, S., Ewertowski, M. and Piekarczyk, J.: Applications of unmanned aerial vehicle (UAV) surveys and Structure from
705 Motion photogrammetry in glacial and periglacial geomorphology, Geomorphology, 378, 107620,
706 doi:10.1016/j.geomorph.2021.107620, 2021.
707 Smith, M. W., Carrivick, J. L. and Quincey, D. J.: Structure from motion photogrammetry in physical geography, Prog. Phys.
708 Geogr., 40(2), 247–275, doi:10.1177/0309133315615805, 2016.
709 Sorg, A., Kääb, A., Roesch, A., Bigler, C. and Stoffel, M.: Contrasting responses of Central Asian rock glaciers to global
710 warming, Sci. Rep., 5(1), 8228, doi:10.1038/srep08228, 2015.

https://doi.org/10.5194/esurf-2021-8
Preprint. Discussion started: 23 February 2021

711 Strozzi, T., Caduff, Jones, Barboux, Delaloye, R., Bodin, Kääb, A., Mätzler and Schrott: Monitoring Rock Glacier Kinematics
712 with Satellite Synthetic Aperture Radar, Remote Sens., 12(3), 559, doi:10.3390/rs12030559, 2020.
713 Swisstopo: swissALTI3D - The high precision digital elevation model of Switzerland, [online] Available from:
714 https://shop.swisstopo.admin.ch/en/products/height_models/alti3D, 2018.
715 Valenzuela, L.: Stability issues in natural and man made slopes in mining, in Landslides: Evaluation and
716 Stabilization/Glissement de Terrain: Evaluation et Stabilisation, Set of 2 Volumes: Proceedings of the Ninth International
717 Symposium on Landslides, edited by W. A. Lacerda, M. Ehrlich, S. A. B. Fontoura, and A. S. F. Sayão, pp. 467–473, Taylor
718 & Francis Group, Rio de Janeiro., 2004.
719 Vautherin, J., Rutishauser, S., Schneider-Zapp, K., Choi, H. F., Chovancova, V., Glass, A. and Strecha, C.: Photogrammetric
720 Accuracy and Modeling of Rolling Shutter Cameras, ISPRS Ann. Photogramm. Remote Sens. Spat. Inf. Sci., III–3(July), 139–
721 146, doi:10.5194/isprsannals-III-3-139-2016, 2016.
722 Villarroel, C. D., Tamburini Beliveau, G., Forte, A., Monserrat, O., Morvillo, M. and Forte, A. P.: DInSAR for a Regional
723 Inventory of Active Rock Glaciers in the Dry Andes Mountains of Argentina and Chile with Sentinel-1 Data, Remote Sens.,
724 10(10), 1588, doi:10.3390/rs10101588, 2018.
725 Vivero, S. and Lambiel, C.: Monitoring the crisis of a rock glacier with repeated UAV surveys, Geogr. Helv., 74(1), 59–69,
726 doi:10.5194/gh-74-59-2019, 2019.
727 Wagner, S.: Creep of alpine permafrost, investigated on the murtel rock glacier, Permafr. Periglac. Process., 3(2), 157–162,
728 doi:10.1002/ppp.3430030214, 1992.
729 Westoby, M. J., Brasington, J., Glasser, N. F., Hambrey, M. J. and Reynolds, J. M.: "Structure-from-Motion" photogrammetry:
730 A low-cost, effective tool for geoscience applications, Geomorphology, 179, 300–314, doi:10.1016/j.geomorph.2012.08.021,
731 2012.
732 Wheaton, J. M., Brasington, J., Darby, S. E. and Sear, D. A.: Accounting for uncertainty in DEMs from repeat topographic
733 surveys: Improved sediment budgets, Earth Surf. Process. Landforms, 35(2), 136–156, doi:10.1002/esp.1886, 2010.
734 Winkler, S. and Lambiel, C.: Age constraints of rock glaciers in the Southern Alps/New Zealand – Exploring their
735 palaeoclimatic potential, Holocene, doi:10.1177/0959683618756802, 2018.
736 Wirz, V., Gruber, S., Purves, R. S., Beutel, J., Gärtner-Roer, I., Gubler, S. and Vieli, A.: Short-term velocity variations at three
737 rock glaciers and their relationship with meteorological conditions, Earth Surf. Dyn., 4(1), 103–123, doi:10.5194/esurf-4-103-
738 2016, 2016.
739

https://doi.org/10.5194/esurf-2021-8
Preprint. Discussion started: 23 February 2021

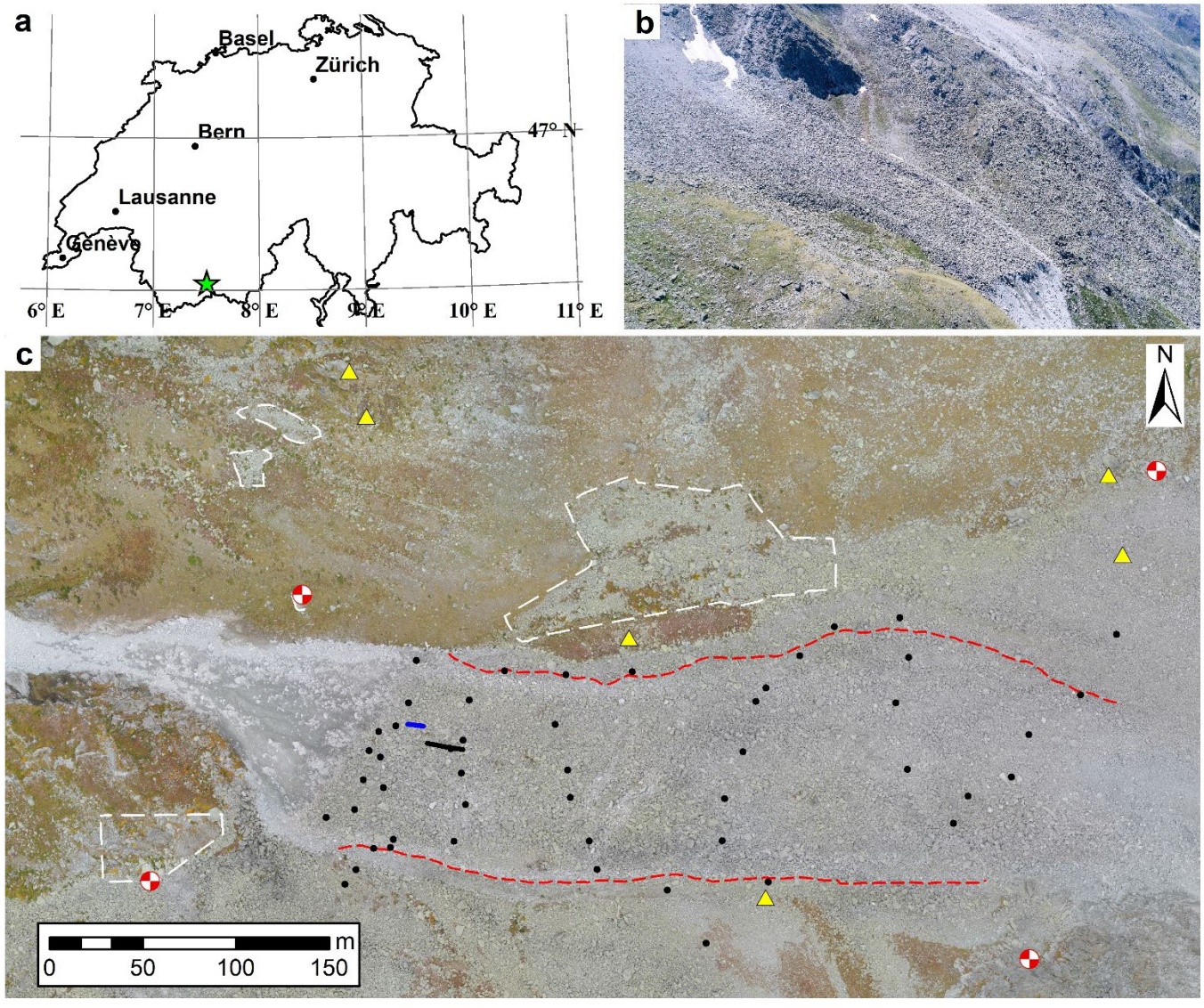

Figure 1. Overview of the Tsarmine rock glacier and its surveying setting. (a) Location of the rock glacier within the Western Swiss Alps (green star). (b) Oblique aerial image from Tsarmine in June 2017. (c) UAV-derived orthomosaic from September 2019. White dashed areas correspond to the stable sectors without the significant vegetation used for coregistration assessments during the image matching step (section 3.3). White and red circles correspond to the GCPs used during each UAV survey. Blue and black lines correspond to the permanent GNSS station trajectories between 2016.01–2017.06 and 2017.06–2020.01, respectively. Red dashed lines correspond to the lateral levees. Black dots and yellow triangles correspond to the rock glacier kinematics and control points (stable points) network, respectively.

https://doi.org/10.5194/esurf-2021-8
Preprint. Discussion started: 23 February 2021

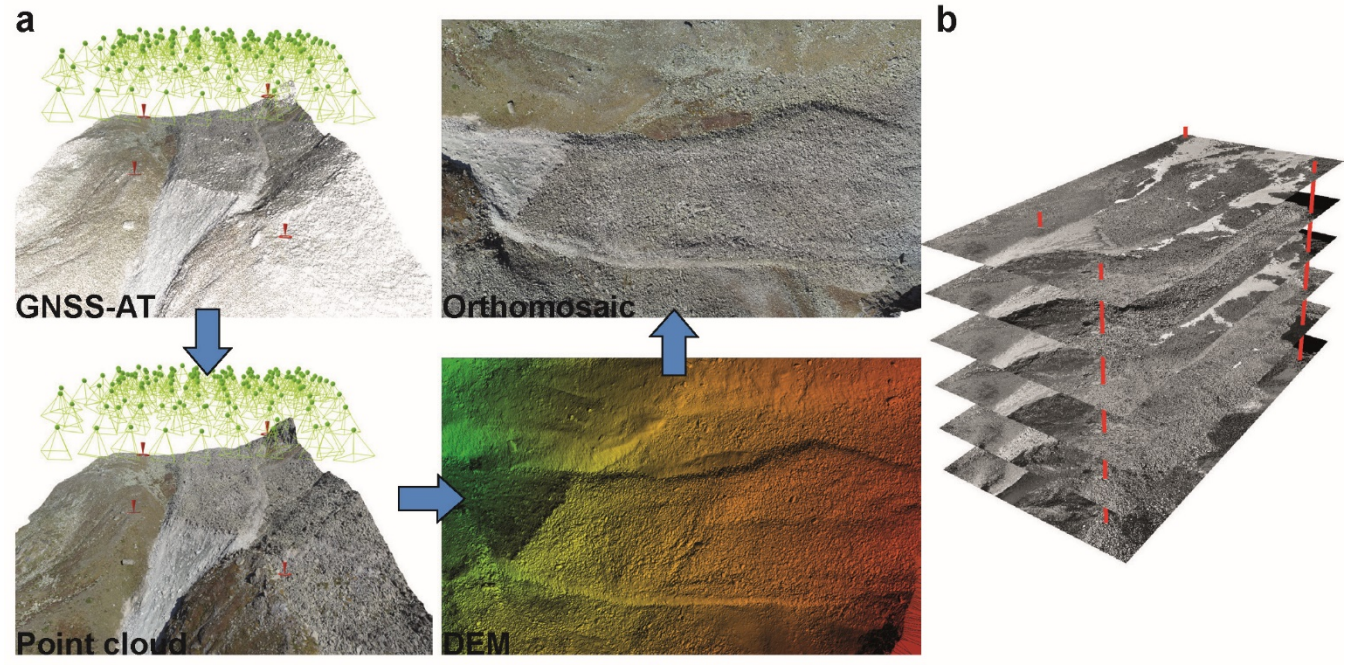

749

750 **Figure 2. (a) SfM processing example from the UAV survey in June 2017. (b) Multitemporal co-registration during the SfM**
751 **processing using four permanent GCP outside the rock glacier.**

https://doi.org/10.5194/esurf-2021-8
Preprint. Discussion started: 23 February 2021

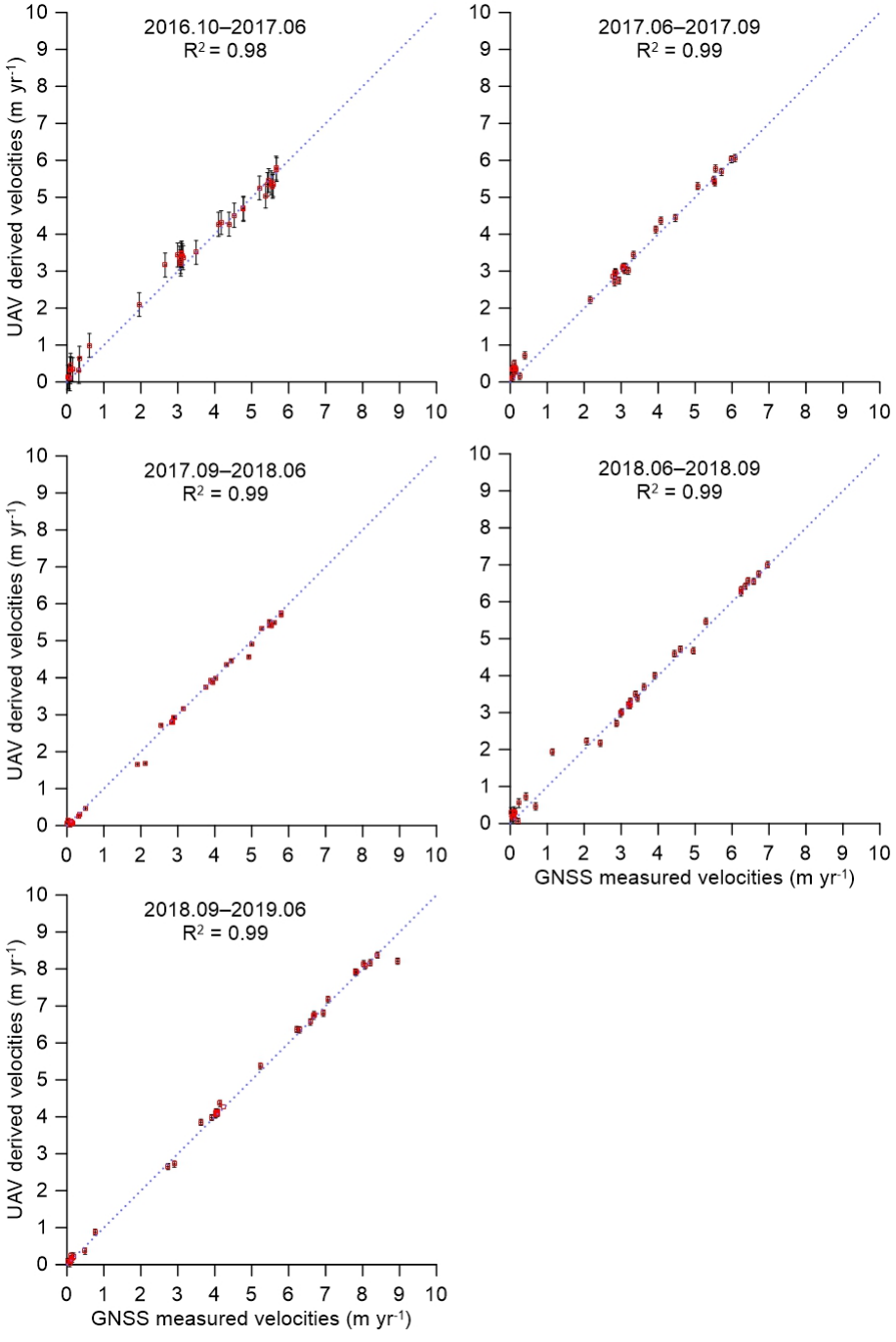

752

753 **Figure 3. Scatterplots of five consecutive periods between velocities derived from UAV analysis and GNSS measurements on 35**
754 **kinematic points. The error bars show the calculated uncertainty for UAV-derived and GNSS measured velocities.**

https://doi.org/10.5194/esurf-2021-8
Preprint. Discussion started: 23 February 2021

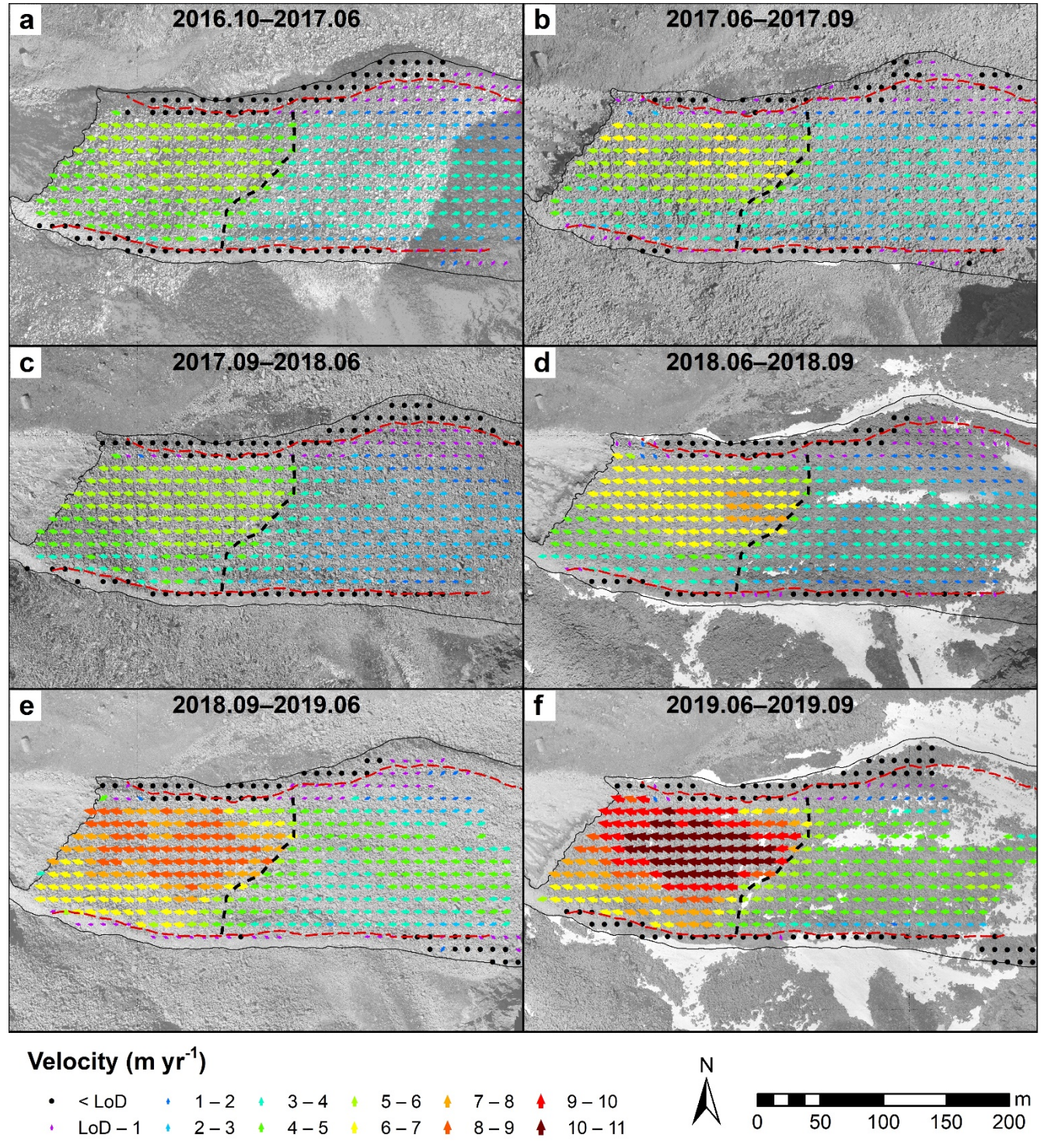

Figure 4. Maps of the horizontal surface velocities between 2016 and 2019. Background images correspond to the first orthomosaic used during each period of image matching. Black dashed lines correspond to the kinematical discontinuity between the lower and upper sections. Red dashed lines correspond to the lateral levees.

https://doi.org/10.5194/esurf-2021-8
Preprint. Discussion started: 23 February 2021

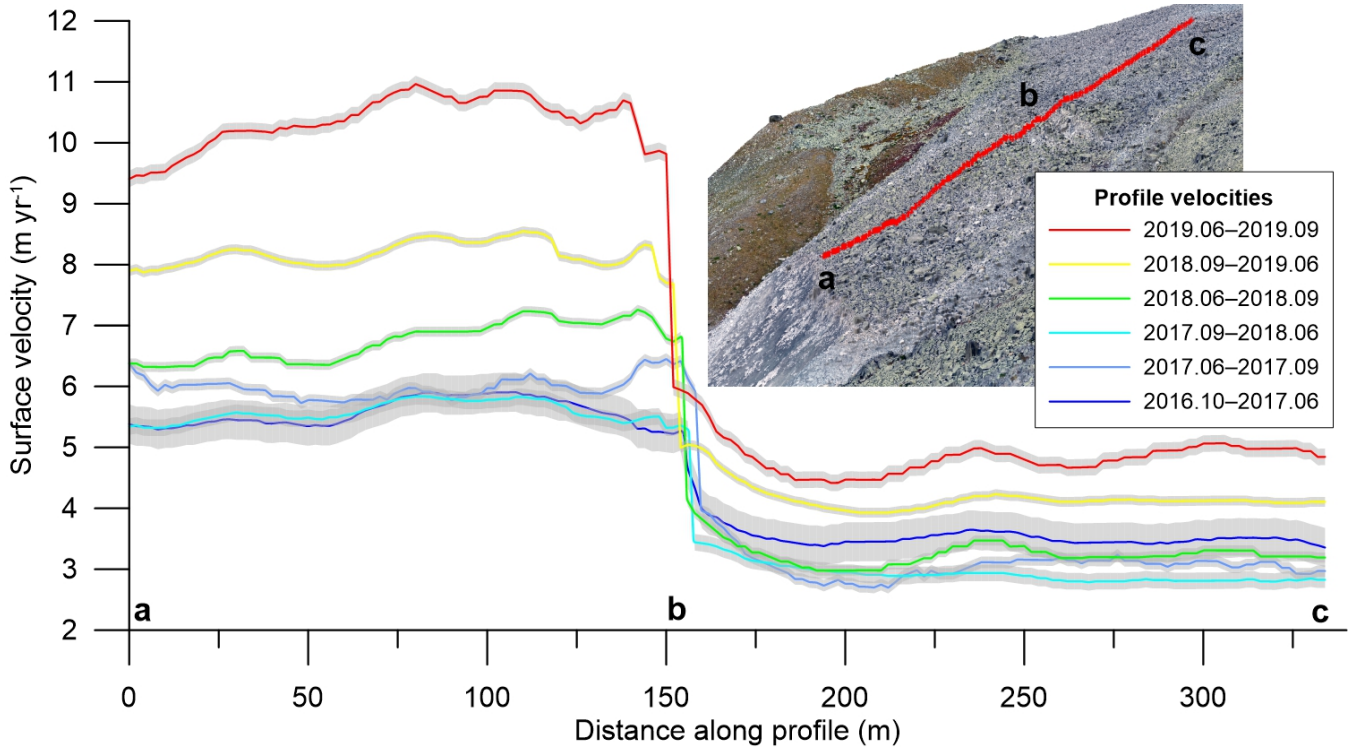

Figure 5. Longitudinal velocity profiles between 2016 and 2019 extracted from the red line shown on the inset. The envelopes display the 90 % confidence level (1.645×σ_l) on for each period.

759

https://doi.org/10.5194/esurf-2021-8
Preprint. Discussion started: 23 February 2021

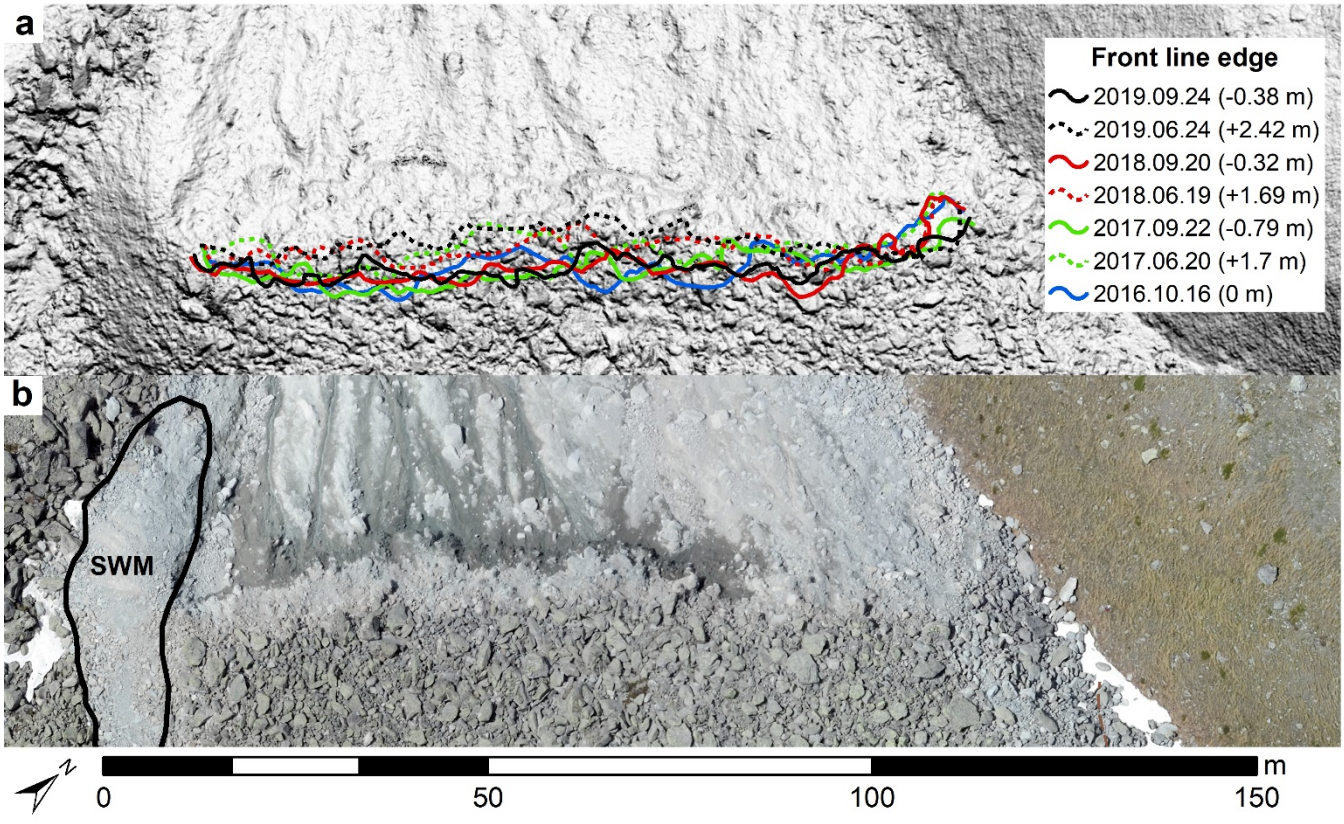

Figure 6. (a) Fluctuations of the front line edge between 2016 and 2019 based on the analysis of the respective orthomosaics. Dashed and continuous lines represent late spring/early summer and late summer/early autumn frontal rock glacier positions, respectively. The mean front line displacements relative to the 2016 position are indicated in parentheses. The background images correspond to a DEM-derived hillshade from June 2019. (b) The delineation of the southwestern margin (SWM) is indicated on the orthomosaic from June 2019 as an example.

https://doi.org/10.5194/esurf-2021-8
Preprint. Discussion started: 23 February 2021

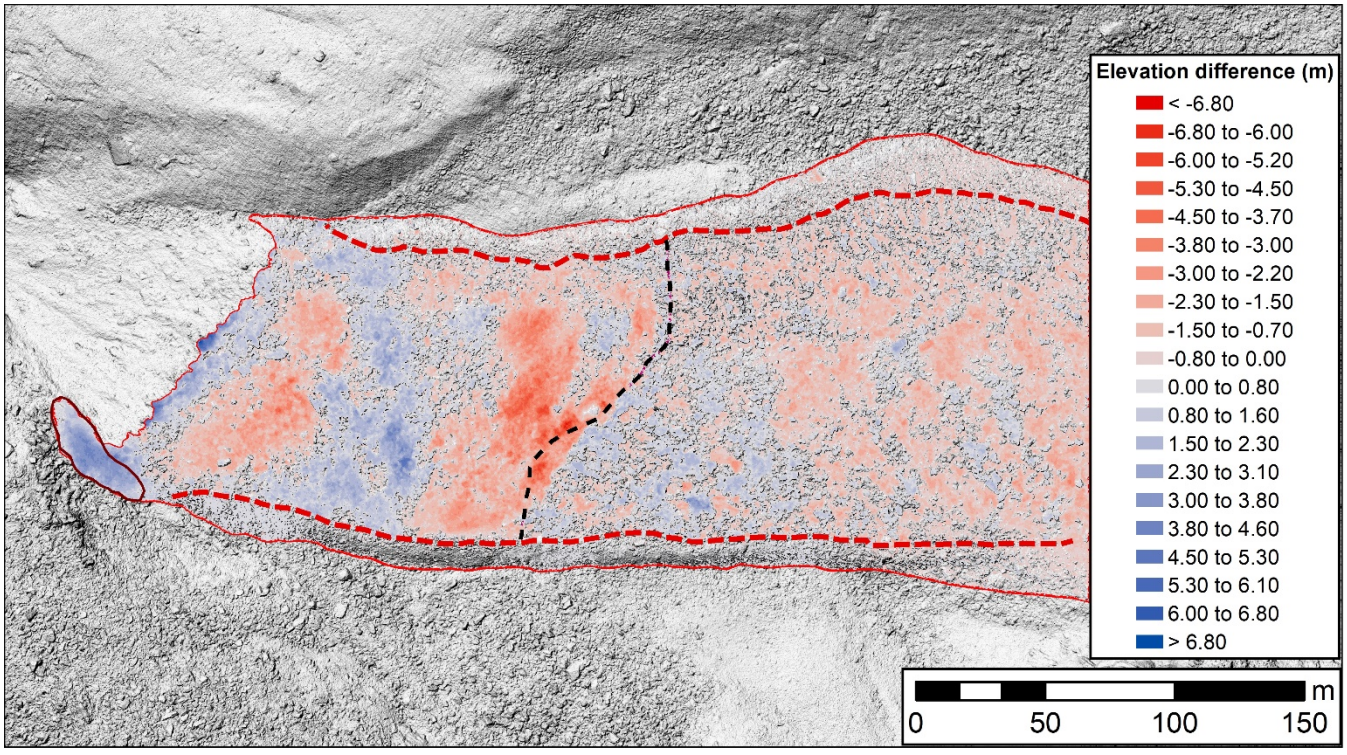

Figure 7. DoD showing the elevation difference for the period 2016-2019. Black and red dashed lines correspond to scarp in 2016 and the lateral levees limits, respectively. The continuous black line indicates the southwestern margin (SWM). The background image corresponds to a DEM-derived hillshade from September 2019.

https://doi.org/10.5194/esurf-2021-8
Preprint. Discussion started: 23 February 2021

Earth Surface Dynamics Discussions
Open Access
EGU

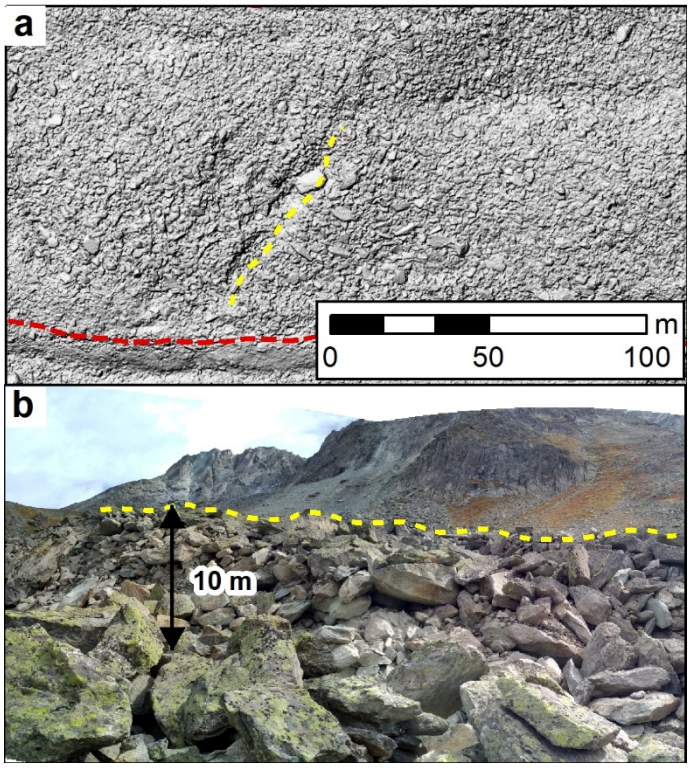

771

772 **Figure 8. (a) Hillshade derived from the 24 September 2019 UAV survey. (b) Photograph acquired during the same day of the UAV**
773 **survey. Yellow and red dashed lines correspond to the scarp's top and the southern lateral levee, respectively.**

774

https://doi.org/10.5194/esurf-2021-8
Preprint. Discussion started: 23 February 2021

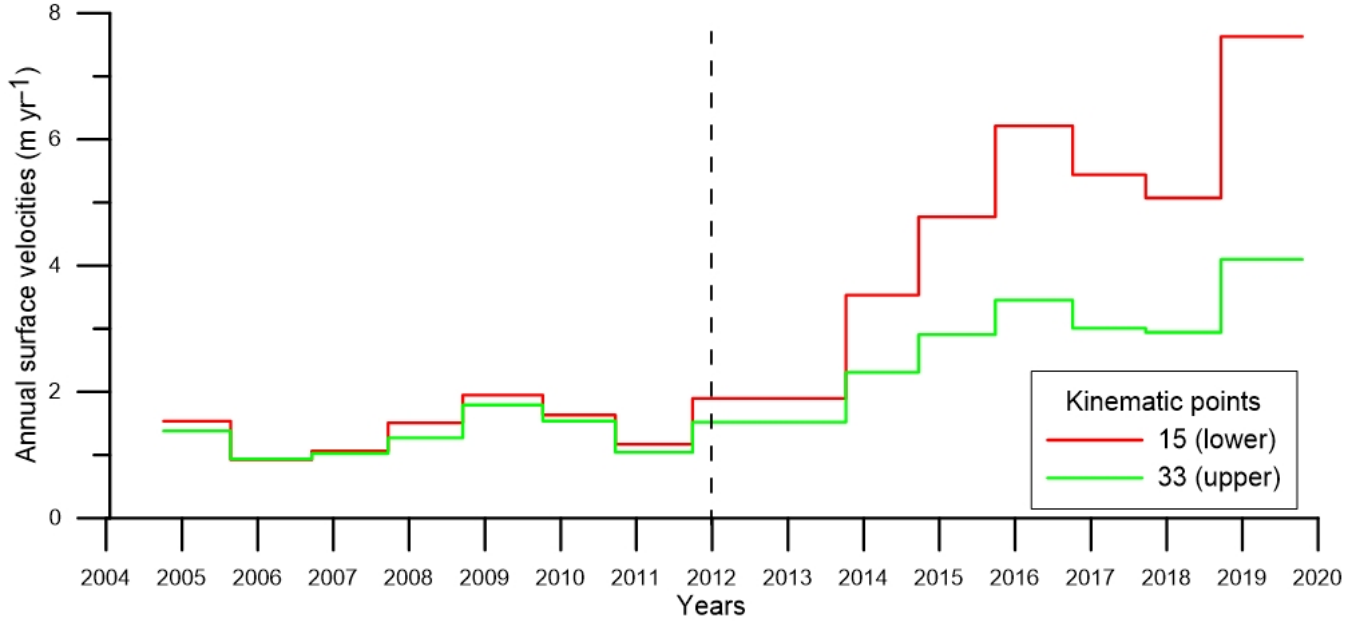

Figure 9. Annual horizontal surface velocities for two kinematics points from 2004 to 2020, representing the behaviour of the lower and upper rock glacier sections (PERMOS, 2019b). Black dashed line suggest the onset of the scarp development.

Table 1. Details of the UAV surveys of Tsarmine rock glacier.

UAV survey	Interval (Days)	Time	Nº Images	Sensor	Average GSD (m)
16 October 2016	-	11:57–12:07	99	SONY WX	0.05
20 June 2017	247	11:49–11:59	97	S.O.D.A.	0.06
22 September 2017	94	13:55–14:09	60	S.O.D.A.	0.08
19 June 2018	270	11:32–11:43	132	S.O.D.A.	0.05
20 September 2018	93	12:59–13:11	149	S.O.D.A.	0.05
24 June 2019	277	13:19–13:50	217	S.O.D.A.	0.05
24 September 2019	92	8:54–9:25	243	S.O.D.A.	0.05

Table 2. Block orientation values using the same four ground control points (GCPs, see Fig.1) and a variable quantity of checkpoints (CPs) located on the rock glacier surface. The RMS error in *x*, *y* and *z* coordinates (in pixel) is indicated for each UAV survey.

UAV survey	GCP RMS *x*	GCP RMS *y*	GCP RMS *z*	Nº CPs	CP RMS *x*	CP RMS *y*	CP RMS z
16 October 2016	0.25	0.14	0.58	-	-	-	-
20 June 2017	0.33	0.40	0.46	5	0.44	0.29	0.88
22 September 2017	0.38	0.19	0.49	3	0.31	0.11	0.40

https://doi.org/10.5194/esurf-2021-8
Preprint. Discussion started: 23 February 2021

19 June 2018	0.30	0.20	0.40	6	0.46	0.26	0.50
20 September 2018	0.35	0.18	0.68	4	0.39	0.21	0.71
24 June 2019	0.22	0.13	0.34	5	0.25	0.18	0.41
24 September 2019	0.20	0.20	0.16	-	-	-	-

783

784 **Table 3. Information on the minimum (Min), maximum (Max) and mean LoD for each period.**

Periods	Min LoD (m)	Max LoD (m)	Mean LoD (m)
2016.10–2017.06	0.31	0.36	0.32
2017.06–2017.09	0.08	0.10	0.09
2017.09–2018.06	0.11	0.13	0.13
2018.06–2018.09	0.08	0.13	0.09
2018.09–2019.06	0.10	0.12	0.10
2019.06–2019.09	0.09	0.14	0.13

785

786 **Table 4. Mean horizontal displacements ($\bar{d}$) and velocities ($\bar{v}$) for the different periods on the lower and upper rock glacier zones.**

Periods	Rock glacier kinematics zones			
	Lower		Upper	
	$\bar{d}$ (m)	$\bar{v}$ (m yr^{-1})	$\bar{d}$ (m)	$\bar{v}$ (m yr^{-1})
2016.10–2017.06	3.40	5.02	2.26	3.34
2017.06–2017.09	1.27	4.93	0.77	2.99
2017.09–2018.06	3.64	4.92	2.09	2.83
2018.06–2018.09	1.40	5.50	0.77	3.02
2018.09–2019.06	5.54	7.30	3.14	4.13
2019.06–2019.09	2.20	8.74	1.12	4.43

787